OPEN ACCESS Freely available online

PLOS | ONE

The Carboxyl-Terminus of Human Immunodeficiency Virus Type 2 Circulating Recombinant form 01_AB Capsid Protein Affects Sensitivity to Human TRIM5α

Tadashi Miyamoto[1], Emi E. Nakayama[1], Masaru Yokoyama[2], Shiro Ibe[3], Shunpei Takehara[1], Ken Kono[1], Yoshiyuki Yokomaku[3], Massimo Pizzato[4], Jeremy Luban[4], Wataru Sugiura[3], Hironori Sato[2], Tatsuo Shioda[1]*

1 Department of Viral Infections, Research Institute for Microbial Diseases, Osaka University, Suita Osaka, Japan, **2** Laboratory of Viral Genomics, Pathogen Genomics Center, National Institute of Infectious Diseases, Musashimurayama, Tokyo, Japan, **3** Department of Infection and Immunology, Clinical Research Center, National Hospital Organization Nagoya Medical Center, Naka-ku, Nagoya, Aichi, Japan, **4** Department of Microbiology and Molecular Medicine, University of Geneva, Geneva, Switzerland

Abstract

Human immunodeficiency virus (HIV) type 2 shows limited geographical distribution compared with HIV type 1. Although 8 genetic groups of HIV type 2 (HIV-2) have been described, recombinant viruses between these groups are rarely observed. Recently, three HIV-2 patients in Japan were described with rapidly progressive, acquired immunodeficiency. These patients were infected with an A/B inter-group recombinant designated CRF01_AB. Here, we characterize the capsid protein (CA) encoded by the viruses from these patients. HIV-2 CRF01_AB CA showed unique amino acid sequence almost equally distinct from group A and group B viruses. Notably, HIV-2 CRF01_AB CA showed potent resistance to human TRIM5α. In addition to the previously identified amino acid position 119 in the N-terminal domain of CA, we found that HIV-2 CRF01_AB-specific amino acid substitutions in the C-terminal domain also were necessary for resistance to human TRIM5α. These results indicate that retroviruses can evade TRIM5α by substitution at residues within the C-terminal domain of CA.

Citation: Miyamoto T, Nakayama EE, Yokoyama M, Ibe S, Takehara S, et al. (2012) The Carboxyl-Terminus of Human Immunodeficiency Virus Type 2 Circulating Recombinant form 01_AB Capsid Protein Affects Sensitivity to Human TRIM5α. PLoS ONE 7(10): e47757. doi:10.1371/journal.pone.0047757

Editor: Vladimir Brusic, Dana-Farber Cancer Institute, United States of America

Received July 31, 2012; **Accepted** September 20, 2012; **Published** October 19, 2012

Funding: This work was supported by grants from the Health Science Foundation; the Ministry of Education, Culture, Sports, Science, and Technology, Japan (23590541 to EEN, 23390111 to TS), the Ministry of Health, Labour, and Welfare, Japan (H22-AIDS-003 to HS), Swiss National Fund grant 3100A0-128655 to JL, and NIH grant RO1AI59159 to JL. The funders had no role in study design, data collection and analysis, decision to publish, or preparation of the manuscript.

Competing Interests: The authors have declared that no competing interests exist.

* E-mail: shioda@biken.osaka-u.ac.jp

Introduction

Human immunodeficiency virus type 2 (HIV-2) has been detected primarily in West Africa, in contrast to the global distribution of the type 1 epidemic virus (HIV-1). Based on molecular evidence, HIV-2 and HIV-1 are presumed to derive from simian immunodeficiency viruses that originated in sooty mangabey (SIVsm) and chimpanzee (SIVcpz), respectively, as a result of zoonotic transfer between non-human primates and human. The HIV-1 and HIV-2 bear a considerable degree of homology in both gene organization and RNA sequence (30%–60%) [1–4]. It is generally believed that HIV-2 is less pathogenic than HIV-1. However, certain HIV-2 patients with high plasma HIV-2 loads develop acquired immune deficiency syndrome (AIDS) as rapidly as HIV-1 patients do [4]. To date, eight HIV-2 groups have been distinguished on the basis of phylogenetic (sequence) analysis; each group is presumed to have originated from an independent zoonotic event [5].

TRIM5α was identified as a factor that restricts HIV-1 infection in rhesus monkey (Rh) cells [6]. TRIM5α is thought to degrade the core of the incoming virus [7,8]. TRIM5 proteins are members of the tripartite motif family containing RING, B-box, and coiled-coil domains. The alpha isoform of TRIM5 has an additional C-terminal PRYSPRY (B30.2) domain [9]. In cynomolgus monkey (CM), TRIM5α also has been demonstrated to restrict HIV-1 infection [6,10]. In contrast, the human TRIM5α exhibits minimal restriction of HIV-1 infection [11–14], but shows moderate levels of restriction for HIV-2 [15].

Capsid (CA) proteins are components of the viral core; the CAs of HIV-1 and HIV-2 have similar primary and three dimensional structures [16]. CA is composed of a surface-exposed N-terminal domain (NTD) and a C-terminal domain (CTD) that is required for oligomerization [17]. We previously identified a single amino acid of the HIV-2 capsid that determines the susceptibility of HIV-2 to CM TRIM5α. Viruses that encoded CAs with either alanine or glutamine at amino acid residue 119 (which corresponded to the 120th amino acid of the CA of the GH123 viral strain) could grow in cells harboring the CM TRIM5α. In contrast, HIV-2 encoding CA with proline at the same position showed restricted growth in cells harboring the CM TRIM5α. Similar results, although to a lesser extent, were observed when the human TRIM5α was used [15]. Furthermore, an analysis of HIV-2 CA variation in a West African Caio cohort demonstrated that the presence of proline at CA positions 119, 159, and 178 was more frequent in individuals with lower viral loads (VLs); the presence of non-proline residues at all 3 residues was more frequent in

individuals with high VLs. The *in vitro* replication levels of viruses bearing changes at the 3 positions suggested that these 3 residues influence virus replication by altering susceptibility to TRIM5α [18]. These results also suggested that TRIM5α controls virus replication in HIV-2-infected individuals.

Recently, five HIV-2-seropositive cases were identified in Japan. Three isolates (NMC307, NMC716, and NMC842) were recovered from these patients and were shown by full-length genomic analysis to represent a recombinant (designated HIV-2 CRF01_AB) of group A and B strains [19]. Although more than 75% of patients with HIV-2 have asymptomatic prognoses throughout their lifetimes [1,20], all 3 of the CRF01_AB patients were found to be at an advanced stage of AIDS with low CD4+ cell counts and high HIV-2 VLs [19]. All 3 patients were under 40 years of age when first diagnosed as HIV-2 positive [19]. Assessment of risk factors suggested that all three were infected via heterosexual contacts; no personal connection was confirmed among any of these cases [19]. In the present study, we characterized the HIV-2 CRF01_AB CA obtained from these patients and found several unique properties of HIV-2 CRF01_AB, including potent resistance to human TRIM5α-mediated restriction.

Results

HIV-2 CRF01_AB Strains Show Unique CA Sequences

Fig. 1 shows an alignment of the deduced amino acid sequences of the CAs of HIV-2 group A (ROD, UC12, GH123, and UC2), HIV-2 group B (UC14, D205, and UC1), SIVs (SIVmac239 and SIVsm PBJ14), and HIV-2 CRF01_AB (NMC307, NMC716, NMC842, and 7312A). As we reported previously [15,18], the 119th amino acid position is a proline, glutamine, or alanine in the CAs of HIV-2 group A, HIV-2 group B, and SIVs. However, the CAs of the HIV-2 CRF01_AB strains uniquely possess a glycine at this position. Based on the genomic structure of HIV-2 CRF01_AB, A/B recombinant breakpoints within this isolate are located near or within the *env* gene, such that HIV-2 CRF01_AB can be considered to consist of a group B backbone that incorporates group A *env* fragments [19]. These presumed breakpoints could be taken to suggest that CRF01_AB CA should be encoded as a B-like sequence. However, phylogenetic analysis of these CA sequences (Fig. 2) reveals that the deduced HIV-2 CRF01_AB CA proteins constitute a distinct cluster, with the dendrogram exhibiting a long branch length compared to the CAs of HIV-2 group A, HIV-2 group B, and SIV.

HIV-2 CRF01_AB CA is Highly Resistant to Human TRIM5α

In a previous study, we reported that the amino acid at residue 119 of the HIV-2 CA affects susceptibility to the restriction of virus replication by CM and human TRIM5α [15], such that HIV-2 encoding CA(Pro119) was sensitive to CM and human TRIM5α, while HIV-2 encoding CA(Gln119) or CA(Ala119) was resistant [15]. We also reported that mutation of HIV-2 strain GH123 to encode glycine at the corresponding position (GH123/G) rendered GH123 resistant to CM TRIM5α [21]. To further test the role of the CA protein in TRIM5α resistance, we generated recombinant versions of the GH123 virus (716 or 842) in which the CA-encoding segment of *gag* was replaced with that of the A/B recombinants NMC716 or NMC842 (respectively). We used a recombinant Sendai virus (SeV) system to express CM, Rh, and human TRIM5α and CM TRIM5α lacking the PRYSPRY domain as a negative control (Fig. S1). In the presence of CM TRIM5α, infection by the parental GH123 virus was restricted, but infection by GH123/G was resistant to CM TRIM5α-mediated restriction (Fig. 3A). Infection by 716 or 842 was resistant to CM TRIM5α (Fig. 3B). In contrast, infection by any of the 4 variants (GH123, GH123/G, 716, and 842) was completely restricted by Rh TRIM5α (Fig. 3A, B). These results for cells producing CM or Rh TRIM5α are consistent with our previous findings [22]. In cells producing human TRIM5α, the replication of parental GH123 and of the GH123/G mutant were partially restricted (Fig. 3A), while 716 and 842 replicated as efficiently as in negative control cells that did not produce a functional TRIM5α (Fig. 3B). The mean ratios of the p25 levels at 6 days after infection in the cells producing human TRIM5α to those in the negative control cells were 0.14 for GH123, 0.30 for GH123/G, but 0.81 for 716 and 1.02 for 842 in three independent experiments. The ratio of GH123/G was significantly higher than that of GH123 ($P = 0.0086$, t test) but lower than those of 716 ($P = 0.0059$, t test) and 842 ($P = 0.0030$, t test). Similar results were obtained when we calculated the mean ratios of the p25 levels at 3 days after infection (data not shown). These data indicate that the CA sequences of the CRF01_AB strains conferred higher potential to escape from human TRIM5α than those of GH123/G.

Viral Sensitivity to Human TRIM5α-mediated Restriction in a Single Round Infection Assay

TRIM5α restricts viral infection at a post-entry step [6,23,24]. To focus on early steps of virus replication, we performed a single-round infection assay, in which infection is detected as fluorescence generated by production of the green fluorescent protein (GFP). To construct mutant viruses encoding GFP, the fragment of GH123, 842, or GH123/G that encoded the matrix (MA) and CA proteins was transferred to the *env*-disrupted HIV-2 genomic clone pROD-env(-)-GFP, which directs the production of GFP after infection [25]. Vesicular stomatitis virus glycoprotein (VSV-G) pseudotyped wild-type and mutant HIV-2 GFP viruses were inoculated into feline CRFK cells producing TRIM5α, and GFP-positive cells were counted 2 days after infection. In this experiment, we used feline cells, since feline cells lack expression of endogenous TRIM5α. In the presence of CM TRIM5α, the numbers of GFP-positive cells were greater in cells infected with GFP-expressing viruses encoding the GH123/G or 842 CAs than in those infected with the GFP-expressing viruses encoding GH123 CA (Fig. 4), confirming that viruses encoding CA(G119) were resistant to CM TRIM5α. Consistent with the results shown in Fig. 3B, the GFP-expressing virus encoding the 842 CA from a patient was more resistant to human TRIM5α-mediated restriction than viruses encoding the CAs from GH123 ($P = 0.0010$, t-test) or GH123/G ($P = 0.0026$, t-test) (Fig. 4).

Viral Growth in TRIM5α Knock-down Cells

We next investigated whether the different resistance to human TRIM5α restriction among recombinant HIV-2 strains still applied in cells producing physiological levels of human TRIM5α protein. For this purpose, we used TRIM5α "knock-down" Jurkat cells (TRIM5α-KD Jurkat) and the corresponding control Jurkat line (Luci-siRNA Jurkat) [26]. It was demonstrated that the level of TRIM5α mRNA in TRIM5α-KD Jurkat is five times lower than that of Luci-siRNA Jurkat by TaqMan quantitative PCR. Three days after infection, GH123 replicated better in TRIM5α-KD Jurkat than in Luci-siRNA Jurkat (Fig. 5A). On the other hand, GH123/G, 716, and 842 yielded comparable titers in both cell lines (Fig. 5B, 5C, and 5D). In this experiment, we found that GH123/G also was resistant to human TRIM5α. Nevertheless, the data presented in Fig. 5 indicated that GH123 was sensitive to human TRIM5α produced at physiologically relevant levels, while 716 and 842 possessed potent resistance against human TRIM5α.

```
HIV-2A  ROD     PVQHVGG-NYTHIPLSPRTLNAWVKLVEEKKFGAEVVPGFQALSEGCTPYDINQMLNCVG  59
        UC1     ...Q.A.-....V.....................................................  59
        GH12    ...QT..G..I.V.............D.....................................  60
        UC2     ...QA..-..V.V.....................................................  59
HIV-2B  UC14    ...QIA.-..S.L.....................................................  59
        D205    ...QLA.-..V.L.....................................................  59
        UC1     ...QIA.-..V.M.....................................................  59
SIV     mac239  ...QI..-..V.L............I.....................................  59
        PBJ14   ...QI..-....L............I.....................................  59
HIV-2AB NMC307  ...Q.A.-..V.V....................I.....................................  59
        NMC716  ...Q.A.-..V.V....................I.....................................  59
        NMC842  ...Q.A.-..V.V....................I.....................................  59
        7312A   ...Q.A.-..V.V.................L.....................................  59

                                                                          119
                                                                           ↓
HIV-2A  ROD     DHQAAMQIIREIINEEAAEWDVQHPIPGPLPAGQLREPRGSDIAGTTSTVEEQIQWMFRP  119
        UC12    .................D.....................................................  119
        GH123   .............D...D..A.............D.....................Y..  120
        UC2     .Q.............D..A.............D.............D......Y.Q  119
HIV-2B  UC14    E.............D..Q...S...M.........................Y.A  119
        D205    E.............D..Q...S...M......D.....................Y.A  119
        UC1     .............D..Q.............D.....................Y.A  119
SIV     mac239  ..........D.......D..L...Q.A.QQ-......S.........S.D......Y.Q  118
        PBJ14   E.............D..L...Q...I.P.................D......Y.Q  119
HIV-2AB NMC307  E......V.........D..Q...V.........D...........P.......Y.G  119
        NMC842  E......V.........D..Q.............D.....................Y.G  119
        NMC716  E......V.........D..Q.............D.....................Y.G  119
        7312A   E......V.........D..Q...V.........D.....................Y.G  119

                                                        159       HindIII  178
                                                         ↓           ↓     ↓
HIV-2A  ROD     QNPVPVGNIYRRWIQIGLQKCVRMYNPTNILDIKQGPKEPFQSYVDRFYKSLRAEQTDPA  179
        UC12    .....................................................................  179
        GH123   ...............................V.....................................  180
        UC2     ............................V..V......S.............A...  179
HIV-2B  UC14    ..............L.....................................................  179
        D205    ..............L.....................................................  179
        UC1     .....................................................................  179
SIV     mac239  ...I..........L.............V.....................A.  178
        PBJ14   ...I..........L.............V.................S.....  179
HIV-2AB NMC307  ..SI..........L.............V.....................A.T.  179
        NMC716  ..S...........L.............V.....................Q.  179
        NMC842  ..S...........L.............V.....................A.T.  179
        7312A   .S.I..........L.............V.....................A.T.  179


HIV-2A  ROD     VKNWMTQTLLVQNANPDCKLVLKGLGMNPTLEEMLTACQGVGGPGQKARLM  230
        UC12    ..........I.............G.....................  230
        GH123   ..........I.....................................  231
        UC2     .....................................................  230
HIV-2B  UC14    ..........I.........................I.........  230
        D205    ..........I.........................I.........  230
        UC1     ..........I.........................I.........  230
SIV     mac239  ..........I.............V.....................  229
        PBJ14   ..........I.............I.....................  230
HIV-2AB NMC307  .RA...E................PH...........I.........  230
        NMC716  .RA...E...I............PH...........I.........  230
        NMC842  .RA...E................PH...........I.........  230
        7312A   .RA...E................PH...........I.........  230
```

Figure 1. Alignments of amino acid sequences of CA proteins encoded by selected HIV-2 isolates and SIV from the Los Alamos databases. Dots denote amino acid identity with the ROD CA; dashes denote gaps introduced to optimize alignment. HIV-2 CRF01_AB-specific amino acid residues are in red. Arrows indicate key residues at 119, 159, and 178, and the position (in the corresponding DNA sequence) of the *Hind*III restriction site used in the constructs. HIV-2A, HIV-2B, and HIV-2AB denote HIV-2 group A, HIV-2 group B, and HIV-2 CRF01_AB, respectively.
doi:10.1371/journal.pone.0047757.g001

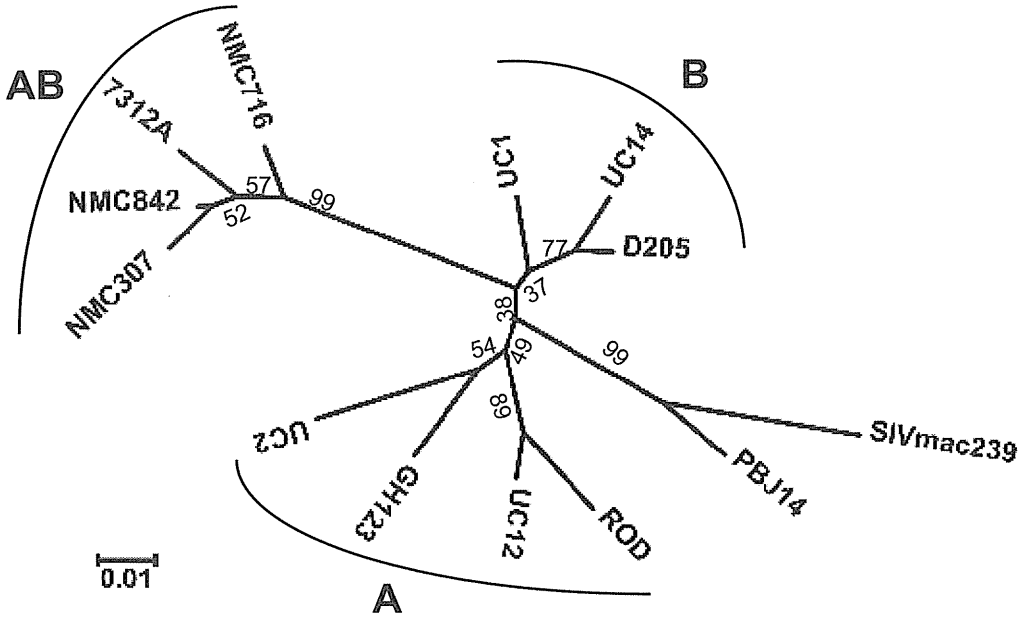

Figure 2. Phylogenetic tree of HIV-2 isolates and SIV. This phylogenetic tree was constructed by the neighbor-joining method. Bootstrap probabilities (%), as calculated by 1000 iterations, are shown at the major tree nodes. Scale bar represents 0.01 amino acid substitutions per site. A, B, and AB denote HIV-2 group A, HIV-2 group B, and HIV-2 CRF01_AB, respectively.
doi:10.1371/journal.pone.0047757.g002

Since TRIM5α-KD Jurkat always showed reduced proliferative properties compared to Luci-siRNA Jurkat (data not shown), presumably due to reduced TRIM5α levels [27], the p25 levels of all these viruses in Luci-siRNA Jurkat became higher than those in TRIM5α-KD Jurkat at 10 days after infection (data not shown).

HIV-2 CRF01_AB CA C-terminal Domain-specific Sequence also Affects Viral Sensitivity to Human TRIM5α

We previously reported that the presence of proline at CA positions 119, 159, and 178 is more frequent in individuals with lower VLs [18]. Viral isolates NMC307, NMC716, and NMC842 all encoded CAs with proline at the 159th position (Fig. 1). However, the 178th amino acid residue was encoded as a threonine (NMC307 and NMC842) or as a glutamic acid (NMC716) in these isolates (Fig. 1). To test whether a single residue at amino acid 178 of HIV-2 CRF01_AB CA affects the sensitivity to human TRIM5α, we generated recombinant 716 or 842 viruses (designated 716GPP or 842GPP, respectively) that encoded CA (Pro178) proteins. As shown in Fig. 3C, 716GPP and 842GPP escaped from human TRIM5α restriction as efficiently as 716 and 842 did. These data suggest the existence of viral determinants for human TRIM5α-resistance other than the previously identified 119th and 178th amino acid positions of CA.

To search for the viral determinants of human TRIM5α resistance other than the 119th and 178th amino acid positions of HIV-2 CA, we constructed a chimeric virus 842Hind by replacing the segment of the 842 genome that encodes CA C-terminal residues 170 to 231 with the corresponding region of GH123 (Fig. 6A). When tested in cells that produced human TRIM5α, 842 was strongly resistant to human TRIM5α as expected (Fig. 6B). However, the 842Hind construct, which encoded the NMC842 CA with the GH123 CA C-terminal short region, lost this resistance to human TRIM5α (Fig. 6C). The mean ratios of the p25 levels at 6 days after infection in the cells producing human TRIM5α to those in the negative control cells were 0.73 for 842 and 0.16 for 842Hind in three independent experiments. The ratio of 842Hind was significantly lower than that of 842 ($P = 0.0003$, t test). Similar results were obtained when we calculated the mean ratios of the p25 levels at 3 days after infection (data not shown). These results suggest that one or more of the HIV-2 CRF01_AB-specific amino acid residues within the CA C-terminal short region (Fig. 1, shown in red) also are necessary to fully evade human TRIM5α.

Molecular Dynamics of N-terminal Domain (NTD) of HIV-2 CRF01_AB CA

Residue 120 of the GH123 CA, which corresponds to residue 119 of the CRF01_AB CA, is located in the loop between α-helices 6 and 7 (L6/7) of CA NTD. Our previous molecular dynamics simulation study of HIV-2 CA NTD revealed that mutations at this position affected conformation of the neighboring loop between α-helices 4 and 5 (L4/5), and TRIM5α-sensitive viruses were predicted to share a common L4/5 conformation. In addition, the shared L4/5 structures of the sensitive viruses were associated with a decreased probability of hydrogen bond formation between GH123 CA's Asp97 (in L4/5) and Arg119 (corresponding to residue 118 in HIV-2 CRF01_AB CA; in L6/7) [21]. TRIM5α-resistant viruses exhibited a variable L4/5 conformation and a higher probability of hydrogen bond formation between L4/5 and L6/7 [21]. As noted above, HIV-2 CRF01_AB strains have a unique Gly119 (Fig. 1), which we had not previously modeled by molecular dynamics simulation. Therefore, three-dimensional (3-D) models of HIV-2 GH123/G and NMC842 CA NTD were constructed using homology modeling based on the crystal structures of the HIV-2 CA NTD, and the models were subjected to molecular dynamics simulation to compare the results with those derived from previously constructed 3-D structural models of TRIM5α-sensitive GH123 and TRIM5α-resistant GH123/Q and GH123/A [21]. GH123/Q and GH123/A encode CA (Gln120) and CA (Ala120), respectively [15]. Contrary to our expectation, the predicted L4/5 conformations of the NTDs of the NMC842 CA and GH123/G CA differed from those of

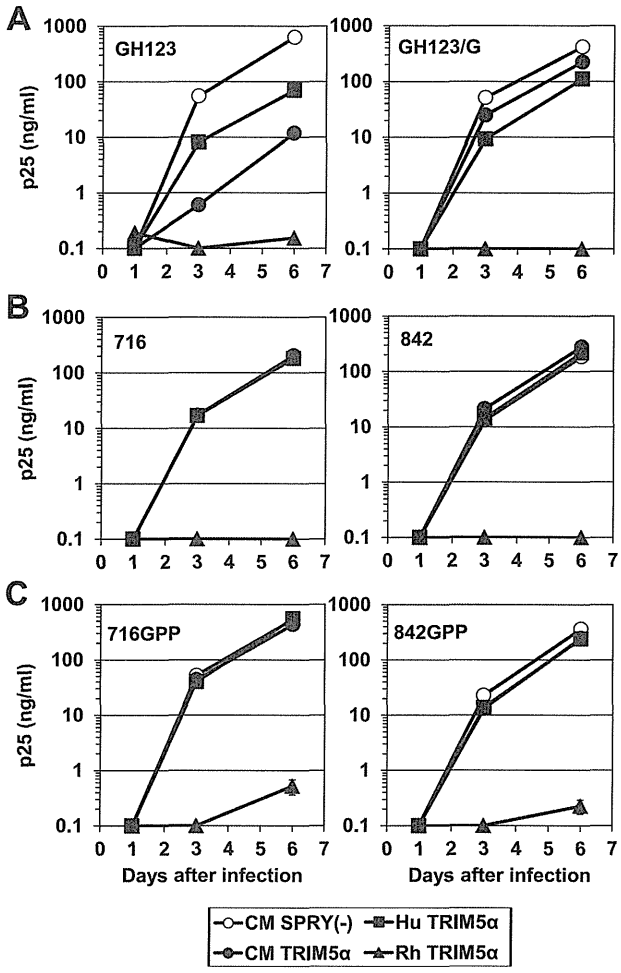

Figure 3. Growth of HIV-2 strain GH123 and variants thereof in the presence of TRIM5α. (A), (B), (C) Virus levels were measured by ELISA detection of p25 (CA) levels in supernatants. CEM-SS cells were infected with recombinant SeV encoding rhesus (Rh: black triangles); cynomolgus monkey (CM: black circles); human (Hu: black squares); or CM SPRY(-) (white circles) TRIM5α. CM SPRY (-) has a dominant negative effect on the anti-viral activity of TRIM5α and serves as a negative control. Nine hours after infection, cells were superinfected with GH123, GH123/G, 716, 842, 716GPP, or 842GPP. Error bars show actual fluctuations between levels of p25 (CA) in duplicate samples from one of three independent experiments.
doi:10.1371/journal.pone.0047757.g003

TRIM5α-resistant GH123/Q and GH123/A, better resembling that predicted for the CA NTD encoded by TRIM5α-sensitive GH123 (Fig. 7). Indeed, the calculated probability of hydrogen bond formation between L4/5 and L6/7 was even lower for the CAs of GH123/G (20.80%) and NMC842 (30.58%) compared to that of GH123 (44.6%). These results suggest that Gly119 endows the CRF01_AB CA NTD with unique structural properties.

Steric Locations of HIV-2 CRF01_AB-specific Amino Acid Substitutions

As noted above, HIV-2 CRF01_AB strains have several specific amino acid substitutions at the C-terminal domain (CTD) of CA (Fig. 1, shown in red); these substitutions were necessary for the potent resistance of these isolates against human TRIM5α (Fig. 6). Previously, we suggested that magnitudes of the computationally calculated binding energies of the CA CTD dimer models tend to be significantly greater in the TRIM5α-less-sensitive HIV-2s in

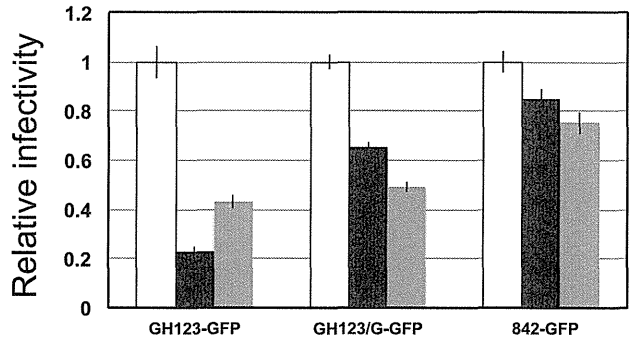

Figure 4. Viral sensitivity to TRIM5α-mediated restriction in a single-round infection assay. Feline CRFK cells were infected with SeV encoding cynomolgus monkey (CM; black bars), human (grey bars), or CM SPRY(-) (white bars) TRIM5α. CM SPRY (-) has a dominant negative effect on the anti-viral activity of TRIM5α and serves as a negative control. The cells then were superinfected with a green fluorescent protein (GFP)-expressing virus, GH123-GFP, GH123/G-GFP, or 842-GFP containing 500ng of p25 (CA). Two days after infection, the cells were fixed by formaldehyde, and GFP-producing cells were counted by flow cytometry. Numbers of GFP-positive cells in CM SPRY (-)-producing cells are set at one and relative numbers to CM SPRY (-) of GFP-positive cells are shown. Error bars denote standard deviations of triplicate samples from one of three independent experiments.
doi:10.1371/journal.pone.0047757.g004

West Africa [18]. To examine if the HIV-2 CRF01_AB-specific amino acid substitutions in CA CTD could influence the CTD-CTD dimer stability, we constructed the CA CTD dimer model of HIV-2 CRF01_AB NMC842 by homology modeling and analyzed steric locations of the specific substitutions and binding energies of the CTD dimer model. In the CA CTD dimer model of NMC842, HIV-2 CRF01_AB-specific amino acid substitutions are located in helix 9 and in the loop between helices 10 and 11, and all appeared to be situated near but distinct from the CTD-CTD dimer interface (Fig. 8A). The predicted binding energy of the CTD-CTD dimer model of the NMC842 isolate (79.6 kcal/mole) was similar to that reported in TRIM5α sensitive viruses [18]. The results may imply that the HIV-2 CRF01_AB-specific amino acid substitutions in CTD do not necessarily influence the CTD-CTD dimer stability of the TRIM5α sensitive virus.

To further obtain structural insights into the roles of these CRF01_AB-specific mutations, we analyzed their steric locations in the CA hexamer. In the hexamer model of GH123 CA that we previously constructed based on the HIV-1 CA hexamer [28], HIV-2 CRF01_AB-specific amino acid substitutions in CTD form clusters and are located at the outermost part of the hexamer (Fig. 8B and C). Notably, these substitutions exist directly under the L4/5 of neighboring CA (Fig. 8C), and most of them are clearly visible from right above (Fig. 8B). These results raise a possibility that HIV-2 CRF01_AB-specific amino acid substitutions in CA CTD may be exposed to and accessible from the outside of the viral core.

Discussion

In the present study, we have shown that the CA of HIV-2 CRF01_AB isolates have a unique feature distinct from that of other HIV-2 strains; CRF01_AB-specific sequences conferred strong resistance to human TRIM5α. In addition to the previously identified role of amino acid 119 of the CA NTD, CRF01_AB-specific amino acid substitutions in the CA CTD also were necessary for strong resistance to human TRIM5α. These amino

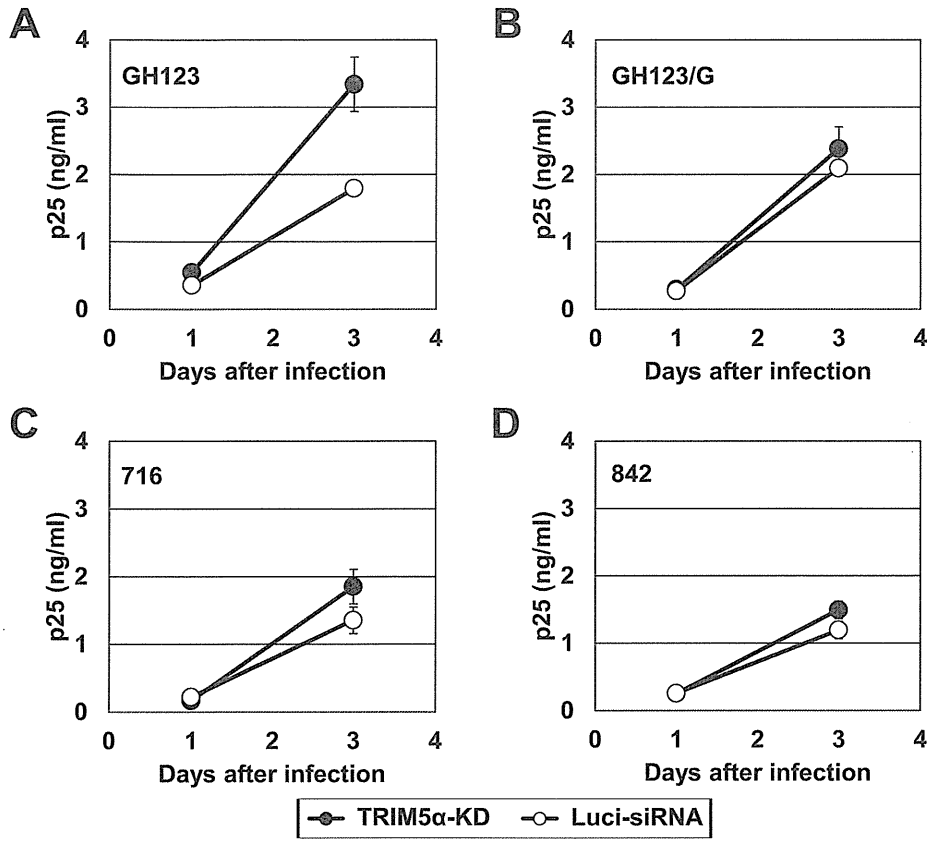

Figure 5. Viral growth in TRIM5α knock-down cells. (A), (B), (C) and (D) TRIM5α-KD Jurkat ("knock-down") or Luci-siRNA Jurkat (control) cells were infected with derivatives of GH123 virus. Culture supernatants were periodically assayed for levels of virus capsid. Error bars show actual fluctuations of duplicate samples from one of two independent experiments. Black and white bars denote TRIM5α-KD Jurkat and Luci-siRNA Jurkat cells, respectively.
doi:10.1371/journal.pone.0047757.g005

acid substitutions in CA CTD may be exposed to and accessible from the outside of the viral core.

Retroviral CA is known to form hexamers [29]. The CTD domain of retroviral capsid protein participates in CA dimerization, where intermolecular CTD-CTD interactions are mediated by symmetric, parallel dimerization of helix 9 from the CTD domains of adjacent hexamers [30]. This dimerization process is prerequisite for assemblies of multiple hexamers [29]. Previously, we found that the computationally calculated binding energies of the CA CTD dimer models could have positive relations with the TRIM5α susceptibilities of HIV-2s in West Africa [18]. We therefore calculated here the binding energy of the CTD-CTD dimer model of the NMC842 using computational method. However, the predicted binding energy of the CTD-CTD dimer of the NMC842 isolate was rather similar to that reported in TRIM5α sensitive viruses [18]. Therefore, previously undescribed mechanisms may be involved in the TRIM5α resistance of the HIV-2 CRF01_AB.

A possible mechanism for the findings may be that the CRF01_AB-specific substitutions influence directly or indirectly the structural properties of an interaction surface for the TRIM5α mediated inhibition. In this regard, we previously suggested with SIV that not only the NTD but also the CTD might constitute an intermolecular interaction surface [31]. Similarly, HIV-2 may have such interaction surface in CTD domain, and the surface may be used for the TRIM5α-mediated inhibition. Results on the steric locations of the CRF01_AB-specific substitutions in the hexamer model support this possibility (Fig. 7B and C). A preliminary modeling study of the assemblies of the CA hexamers also have supported this possibility: the NTDs are apart from each other among the hexamers, which allows to form accessible surface on the CTDs (data not shown), as suggested with Rous sarcoma virus CA [32]. Therefore, it would be interesting to examine whether HIV-2 CRF01_AB-specific amino acid substitutions in CTD could constitute a binding cleft for the TRIM5α itself or others involved in TRIM5α medicated inhibition in the assemblies of multiple CA hexamers in the viral core. Further study is necessary to address this issue.

Previously, we showed that the amino acid replacements at CA residue 119 affected the conformation of the neighboring L4/5, and that TRIM5α-sensitive viruses had a shared L4/5 conformation that was associated with a decreased probability of hydrogen bonding between L4/5 and L6/7 [21]. Although GH123/G and 842 showed resistance to TRIM5α, the calculated probability of hydrogen bond formation between L4/5 and L6/7 was lower than that calculated for the CAs of other TRIM5α-resistant viruses, including that from GH123/Q (55.15%) and GH123/A (64.47%) [21]. The conformations of L4/5 in the CAs of GH123/G and 842 also were similar to those of TRIM5α-sensitive viruses, and were distinct from those of the CAs of TRIM5α-resistant viruses. These characteristics of GH123/G and 842 were similar to those of GH123/E and GH123/D, mutant GH123 clones encoding glutamic acid and aspartic acid (respectively) at the residue corresponding to

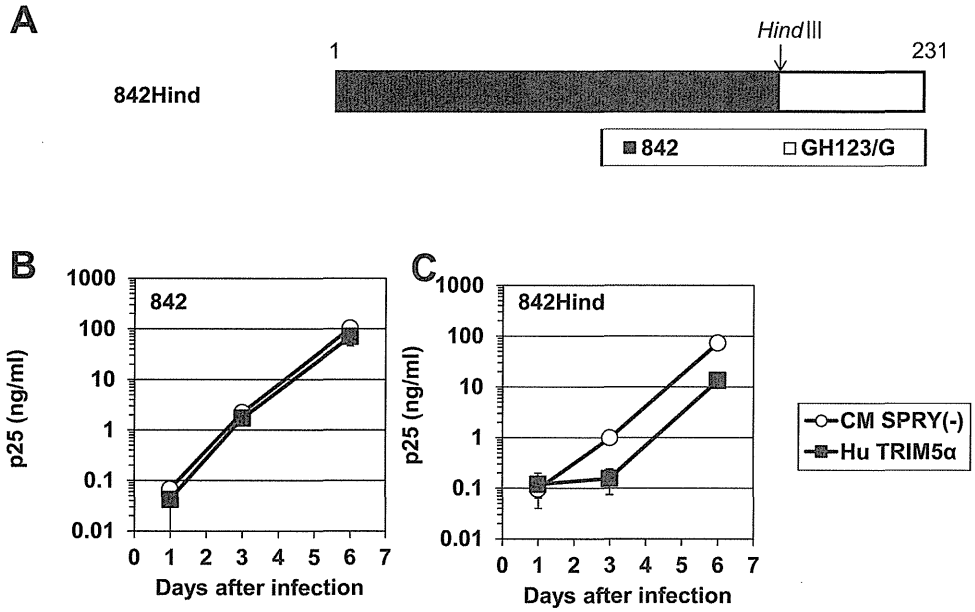

Figure 6. HIV-2 CRF01_AB CA C-terminal domain-specific sequence also affects viral sensitivity to human TRIM5α. (A) Schematic representation of chimeric viral CAs. Black and white bars show 842 and GH123/G CA peptide sequences, respectively. An arrow denotes the position (in the corresponding DNA sequence) of the *Hind*III restriction site used in the construct. (B and C) CEM-SS cells were infected with recombinant SeV encoding human (Hu: black squares) or CM SPRY(-) (white circles) TRIM5α. Nine hours after infection, cells were superinfected with 842 (B) and 842Hind (C). Culture supernatants were assayed for levels of p25 (CA). Error bars show actual fluctuations between levels of p25 (CA) in duplicate samples from one of three independent experiments.
doi:10.1371/journal.pone.0047757.g006

position 119 of HIV-2 CRF01_AB strains [21]. Although glutamic acid and aspartic acid have not been observed at this CA residue in HIV-2 isolated clinically, both GH123/E and GH123/D showed resistance against CM TRIM5α. In contrast to the CAs of GH123/Q and GH123/A, the CAs of both GH123/E and GH123/D show reduced likelihoods of hydrogen bond formation between the L4/5 and L6/7, and the L4/5 conformations were predicted to be similar to those of the CAs of TRIM5α-sensitive viruses. Therefore, our present results extend our previous observations, and additionally imply that the Gly119 of HIV-2 CRF01_AB CA prevents binding by TRIM5α, probably due to the small size of the glycine side chain. It is possible that the shared conformation of L4/5 might have some advantages in utilizing certain cellular factor(s) that bind CA. Our structural data suggests that HIV-2 CRF01_AB strains are highly adapted, since these strains have acquired potent resistance against TRIM5α without losing the shared L4/5 conformation.

In the case of GH123/E, disruption of the hydrogen bond between L4/5 and L6/7 by substitution of alanine for aspartic acid at position 97 (D97A) did not alter the resistant phenotype of GH123/E [21], while the same substitution almost completely abolished the replicative ability of GH123/G (data not shown). This result further demonstrates the unique status of GH123/G, since D97A substitution did not cause such a drastic reduction of replicative ability in GH123, GH123/Q, and GH123/A [21]. The basis for the difference between GH123/G and other variants is unclear; further mutational studies will be necessary to elucidate detailed interactions between L4/5 and L6/7, and to define the contribution of these sequences to viral replication and TRIM5α sensitivity.

In the Los Alamos databases, almost all SIV isolates encode glutamine at the position corresponding to residue 119 of the HIV-2 CRF01_AB CA. It is likely that the sequential mutation from glutamine (coded as CAA or CAG) to proline (CCA or CCG; underlines denote single nucleotide changes) and then to alanine (GCA, GCG) occurred after transmission of the monkey virus to the human population. The nature of the genetic code suggests that the Gly119-encoding virus (GGA or GGG codon) derived from the Ala119-encoding virus, implying that the viruses with glycine are highly adapted, as also discussed above. A single HIV-2 strain encoding glycine at the 119th CA residue was found in the Los Alamos databases; this strain (7312A) was isolated from a symptomatic 32-years-old man [33], and also was a recombinant between groups A and B (Fig. 1 and 2). This recombinant virus exhibits a genomic organization similar to that of NMC307, NMC716, and NMC842. At present, we do not know whether the emergence of glycine at the 119th position of CA is unique to HIV-2 CRF01_AB. It will be critical to assess the emergence of Gly119 viruses within HIV-2 groups A and B.

It is generally believed that HIV-2 is less pathogenic than HIV-1, and the number of HIV-2 cases is now gradually decreasing in West Africa. However, NMC307, NMC716, and NMC842 were recovered from patients at an advanced stage of AIDS with low CD4+ cell counts and high HIV-2 VLs [19]. It is possible that these HIV-2 CRF01_AB strains are highly pathogenic, unlike other HIV-2 strains. Careful epidemiological and virological studies are necessary to test this hypothesis. In the present study, we found that HIV-2 CRF01_AB CA confers strong resistance to human TRIM5α. In the Caio HIV-2 cohort in West Africa, non-proline residues at position 119 were significantly associated with elevated plasma HIV-2 load [18]. Therefore, resistance to TRIM5α may at least partially explain why these 3 patients in Japan developed AIDS so rapidly, although the possible effects of mutations in regions (e.g., *env*, *vif*, *nef* and the long terminal repeats) other than those that encode CA cannot be fully excluded at

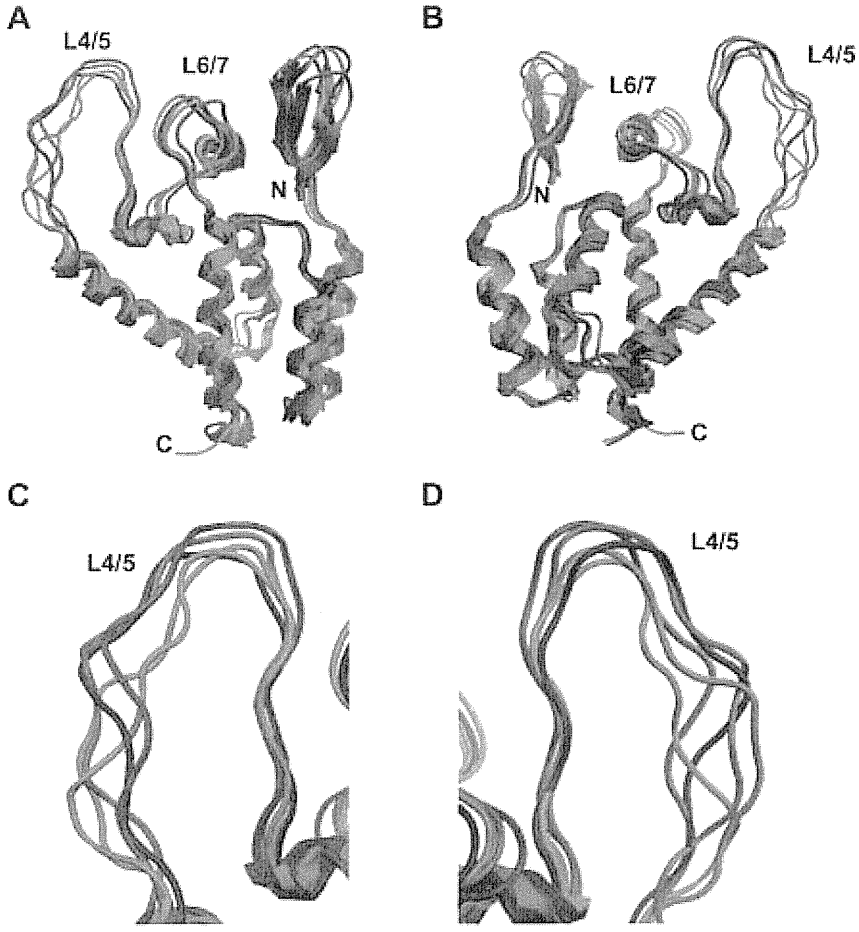

Figure 7. Structural models of the HIV-2 capsid N-terminal domain. Models were constructed by homology modeling and molecular dynamics simulations with the high-resolution X-ray crystal structure of the HIV-2 capsid N-terminal domain (CA NTD) (PDB code: 2WLV [16]) as the starting structure. Averaged conformations of the overall structure of the CA NTD (from the amino acid position 1 to 150) during 5–20 nanoseconds of MD simulations (A and B) and a close-up view around the L4/5 loop (C and D) are indicated. N and C indicate the amino termini and carboxyl termini, respectively. Models are color coded as follows: red, 842; blue, GH123/G; green, CM TRIM5α-resistant viruses (GH123/Q and GH123/A); and purple, CM TRIM5α-sensitive virus (GH123/P).
doi:10.1371/journal.pone.0047757.g007

present. Our results also suggest that resistance to TRIM5α might be a new marker for the pathogenic potential of HIV-2. The possible emergence of a highly pathogenic HIV-2 strain is an ongoing concern, given that retroviruses can easily evolve to evade host defenses.

Materials and Methods

Phylogenetic Tree Analysis

Multiple sequence alignment was performed using the software CLUSTALW version 2.1. Phylogenetic trees were constructed using the neighbor-joining method. Bootstrap probabilities were calculated by 1000 iterations [34].

Cell Culture

The human 293T [35] and feline CRFK [36] cells were maintained in Dulbecco's Modified Eagle medium. The human T-cell line CEM-SS [37] was maintained in RPMI medium. All media were supplemented with 10% fetal bovine serum and 1% penicillin-streptomycin.

Plasmid Construction

Recombinant HIV-2 GH123 clones containing the entire CA sequence of the isolates NMC716 or NMC842 (716 or 842, respectively) and 716 or 842 with proline substitutions at the 178th position (716GPP or 842GPP, respectively) were generated by PCR-based mutagenesis. The GH123/G virus was described previously [21]. The 0.6-kb *Hind*III-*Xho*I fragment of 842 was replaced with the corresponding fragment of GH123/G, and the resulting plasmid was designated 842Hind. Infectious viruses were prepared by transfection of 293T cells with the resulting proviral DNA clones. Viral titers were determined by measuring P25 (CA) with a RetroTek antigen ELISA kit (ZeptoMetrix, Buffalo, NY).

To construct the wild-type and mutant HIV-2 clones encoding GFP, the 1.6-kb *Kpn*I-*Xho*I fragment (which encodes the MA, CA and p6) of GH123, 842, or GH123/G, was transferred to pROD-env(-)-GFP [25], a clone in which the *env* gene is disrupted, and the GFP gene was inserted into the *nef* region. Infectious viruses were prepared by transfection of 293T cells with proviral DNA clones together with the pMD2G plasmid encoding VSV-G. Viral titers were determined as above.

Construction of recombinant SeV encoding C-terminally HA-tagged CM TRIM5α (CM-TRIM5α-SeV), Rh TRIM5α (Rh-

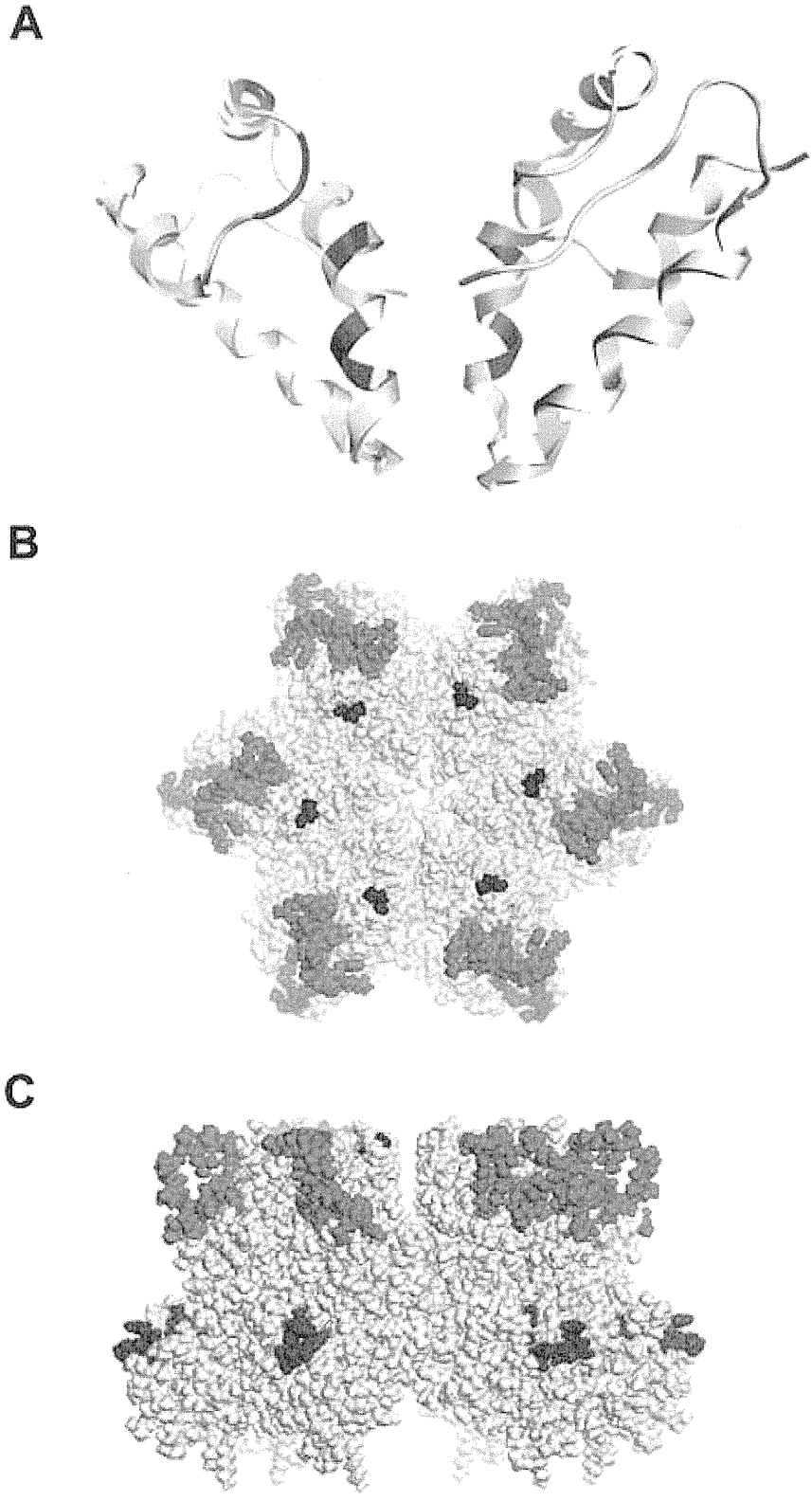

Figure 8. Structural models of the HIV-2 capsid C-terminal domain in dimeric form (A) and the HIV-2 GH123 capsid hexamer (B and C). (A) The C-terminal domain dimer model (from the amino acid position 150 to 219) of HIV-2 capsid (CA) is based on the viral sequence of NMC842. HIV-2 CRF01_AB-specific amino acid substitutions are shown in red. (B and C) The space-filling model of CA hexamer from the top (B) and side (C) is shown. Positions of HIV-2 CRF01_AB-specific amino acid substitutions are shown in red. L4/5 and 120P are shown in green and blue, respectively.
doi:10.1371/journal.pone.0047757.g008

TRIM5α-SeV), human TRIM5α (Hu-TRIM5α-SeV), and CM TRIM5α lacking the PRYSPRY domain (CM-SPRY(-)-SeV) were described previously [10,15,22].

Viral Infection

CEM-SS cells (1×10^6) were infected with SeVs encoding the respective TRIM5α proteins at a multiplicity of infection of 10 plaque-forming units per cell and incubated at 37°C for 9 h. Aliquots of 1×10^5 cells were then superinfected with GH123, GH123/G, 716, 716GPP, 842, 842GPP, or 842Hind virus. Each superinfection used a titer of virus corresponding to 20 ng of p25 (CA). Experiment was performed three separate times with duplicate samples. For viral infection of cells producing physiological levels of TRIM5α, TRIM5α knock-down Jurkat cells (TRIM5α-KD Jurkat) and control cells (Luci-siRNA Jurkat) were infected with GH123, GH123/G, 716, or 842 virus. Each infection used a titer of virus corresponding to 100 ng of p25. The culture supernatants were collected periodically, and the level of p25 (CA) was measured as described above. Experiment was performed two separate times with duplicate samples.

Western Blot

CEM-SS cells (1×10^6) infected with recombinant SeVs expressing HA-tagged TRIM5α proteins were lysed in lysis buffer (50 mM Tris-HCl, pH 7.5, 150 mM NaCl, 1% Nonidet P40, 0.5% sodium deoxycholate). TRIM5α proteins in the lysates were subjected to sodium dodecyl sulfate-polyacrylamide gel electrophoresis. Proteins in the gel were then electronically transferred onto a membrane (Immobilon; Millipore, Billerica, MA). Blots were blocked and probed with anti-HA high-affinity rat monoclonal antibody (Roche, Indianapolis, IN) overnight at 4°C. Blots were then incubated with peroxidase-conjugated anti-rat IgG (American Qualex, San Clemente, CA), and bound antibodies were visualized with a Chemilumi-One chemiluminescent kit (Nacalai Tesque, Kyoto, Japan).

Single-round Infection Assay

SeV-infected CRFK cells (4×10^4) were infected with a titer of pROD-env(-)-GFP derivative virus corresponding to 500 ng of p25 (CA). Two days after infection, the cells were fixed by formaldehyde, and GFP-producing cells were counted by flow cytometry. Experiment was performed three separate times with triplicate samples.

Molecular Modeling and MD Simulation

We used molecular dynamic (MD) simulations [38] to analyze the structural dynamics of the HIV-2 CA NTDs. First, initial CA structures for MD simulation were constructed by homology modeling [39] using the Molecular Operating Environment, MOE (Chemical Computing Group Inc., Montreal, Canada) as described previously [15,40]. We used the high-resolution crystal structure of the HIV-2 CA NTD at a resolution of 1.25Å (PDB code: 2WLV) [16] as the modeling template. Structural dynamics of these HIV-2 CA models in an aqueous environment were analyzed using MD simulations with the SANDER module in the AMBER 9 program package [41] and the AMBER99SB force field with the TIP3P water model [42]. Bond lengths involving hydrogen were constrained with SHAKE [43] and the time step for all MD simulations was set to 2 fs. After heating calculations for 20 ps to 310 K using the NVT ensemble, the simulations were executed using the NPT ensemble at 1 atm and 310 K for 20 ns. Hydration analyses were performed using the ptraj module in AMBER. A maximum cut-off angle of 120.0° and cut-off length of 3.5 Å were used in hydrogen bond definitions.

For the CTD dimer model of HIV-2 CRF01_AB NMC842, a crystal structure of the HIV-1 CA protein was used as the template for the modeling; the dimer of CA C-terminal domain at a resolution of 1.70 Å (PDB code: 1A8O) [17]. The amino acid sequence identity of HIV-1 (1A8O) and HIV-2 CA (NMC842 in this study) is about 76%. The sequence similarity is sufficient to construct a structural model with an r.m.s. deviation of approximately 1.5 Å for the main chain between the predicted and actual structures [39]. The 3-D structures were optimized thermodynamically by energy minimization using MOE and an AMBER99 force field [44] and further refined the physically unacceptable local structures on the basis of evaluation of unusual dihedral angles, *phi* and *psi*, by the Ramachandran plot using MOE. The binding energies of the CA dimer models, E_{bind}, were calculated as described elsewhere [45,46], using the formula $E_{bind} = E_{dimer} - 2E_{monomer}$, where E_{dimer} is the energy of the CA dimer; $E_{monomer}$ is the energy of the CA monomer.

Conclusions

The CA of HIV-2 CRF01_AB isolates have a unique feature distinct from that of other HIV-2 strains; CRF01_AB-specific sequences conferred strong resistance to human TRIM5α. CRF01_AB-specific amino acid substitutions in the CA CTD were necessary for strong resistance to human TRIM5α.

Supporting Information

Figure S1 Western blot analysis of TRIM5α proteins. HA-tagged TRIM5α proteins in lysate of CEM-SS cells infected with recombinant SeV were visualized by western blotting with an antibody against HA. S(-), Hu, CM, and Rh denote CM SPRY(-), human, cynomolgus monkey, and rhesus TRIM5α, respectively. Molecular weight makers are shown on the left.
(EPS)

Acknowledgments

We thank Dr. Y. Tian, Dr. S. Nakamura and Dr. T. Yasunaga for helpful discussions, and Ms. S. Bando and Ms. N. Teramoto for assistance.

Author Contributions

Conceived and designed the experiments: TM EEN SI HS TS. Performed the experiments: TM EEN MY ST KK. Analyzed the data: TM EEN MY SI KK JL WS HS TS. Contributed reagents/materials/analysis tools: SI YY MP JL WS. Wrote the paper: TM EEN MY SI JL HS TS.

References

1. Rowland-Jones SL, Whittle HC (2007) Out of Africa: what can we learn from HIV-2 about protective immunity to HIV-1? Nat Immunol 8: 329–331.
2. Gao F, Bailes E, Robertson DL, Chen Y, Rodenburg CM, et al. (1999) Origin of HIV-1 in the chimpanzee Pan troglodytes troglodytes. Nature 397: 436–441.
3. Huet T, Cheynier R, Meyerhans A, Roelants G, Wain-Hobson S (1990) Genetic organization of a chimpanzee lentivirus related to HIV-1. Nature 345: 356–359.
4. Gottlieb GS, Sow PS, Hawes SE, Ndoye I, Redman M, et al. (2002) Equal plasma viral loads predict a similar rate of CD4+ T cell decline in human immunodeficiency virus (HIV) type 1- and HIV-2-infected individuals from Senegal, West Africa. J Infect Dis 185: 905–914.
5. Damond F, Worobey M, Campa P, Farfara I, Colin G, et al. (2004) Identification of a highly divergent HIV type 2 and proposal for a change in HIV type 2 classification. AIDS Res Hum Retroviruses 20: 666–672.
6. Stremlau M, Owens CM, Perron MJ, Kiessling M, Autissier P, et al. (2004) The cytoplasmic body component TRIM5alpha restricts HIV-1 infection in Old World monkeys. Nature 427: 848–853.

7. Sebastian S, Luban J (2005) TRIM5alpha selectively binds a restriction-sensitive retroviral capsid. Retrovirology 2: 40.
8. Stremlau M, Perron M, Lee M, Li Y, Song B, et al. (2006) Specific recognition and accelerated uncoating of retroviral capsids by the TRIM5alpha restriction factor. Proceedings of the National Academy of Sciences of the United States of America 103: 5514–5519.
9. Reymond A, Meroni G, Fantozzi A, Merla G, Cairo S, et al. (2001) The tripartite motif family identifies cell compartments. Embo J 20: 2140–2151.
10. Nakayama EE, Miyoshi H, Nagai Y, Shioda T (2005) A specific region of 37 amino acid residues in the SPRY (B30.2) domain of African green monkey TRIM5alpha determines species-specific restriction of simian immunodeficiency virus SIVmac infection. Journal of Virology 79: 8870–8877.
11. Hatziioannou T, Perez-Caballero D, Yang A, Cowan S, Bieniasz PD (2004) Retrovirus resistance factors Refl and Lv1 are species-specific variants of TRIM5alpha. Proceedings of the National Academy of Sciences of the United States of America 101: 10774–10779.
12. Keckesova Z, Ylinen LM, Towers GJ (2004) The human and African green monkey TRIM5alpha genes encode Refl and Lv1 retroviral restriction factor activities. Proceedings of the National Academy of Sciences of the United States of America 101: 10780–10785.
13. Perron MJ, Stremlau M, Song B, Ulm W, Mulligan RC, et al. (2004) TRIM5alpha mediates the postentry block to N-tropic murine leukemia viruses in human cells. Proceedings of the National Academy of Sciences of the United States of America 101: 11827–11832.
14. Nakayama EE, Shioda T (2010) Anti-retroviral activity of TRIM5 alpha. Rev Med Virol 20: 77–92.
15. Song H, Nakayama EE, Yokoyama M, Sato H, Levy JA, et al. (2007) A single amino acid of the human immunodeficiency virus type 2 capsid affects its replication in the presence of cynomolgus monkey and human TRIM5alphas. Journal of Virology 81: 7280–7285.
16. Price AJ, Marzetta F, Lammers M, Ylinen LM, Schaller T, et al. (2009) Active site remodeling switches HIV specificity of antiretroviral TRIMCyp. Nat Struct Mol Biol 16: 1036–1042.
17. Gamble TR, Yoo S, Vajdos FF, von Schwedler UK, Worthylake DK, et al. (1997) Structure of the carboxyl-terminal dimerization domain of the HIV-1 capsid protein. Science 278: 849–853.
18. Onyango CO, Leligdowicz A, Yokoyama M, Sato H, Song H, et al. (2010) HIV-2 capsids distinguish high and low virus load patients in a West African community cohort. Vaccine 28S2: B60–B67.
19. Ibe S, Yokomaku Y, Shiino T, Tanaka R, Hattori J, et al. (2010) HIV-2 CRF01_AB: first circulating recombinant form of HIV-2. J Acquir Immune Defic Syndr 54: 241–247.
20. Marlink R, Kanki P, Thior I, Travers K, Eisen G, et al. (1994) Reduced rate of disease development after HIV-2 infection as compared to HIV-1. Science 265: 1587–1590.
21. Miyamoto T, Yokoyama M, Kono K, Shioda T, Sato H, et al. (2011) A single amino acid of human immunodeficiency virus type 2 capsid protein affects conformation of two external loops and viral sensitivity to TRIM5alpha. PloS one 6: e22779.
22. Kono K, Song H, Shingai Y, Shioda T, Nakayama EE (2008) Comparison of anti-viral activity of rhesus monkey and cynomolgus monkey TRIM5alphas against human immunodeficiency virus type 2 infection. Virology 373: 447–456.
23. Wu X, Anderson JL, Campbell EM, Joseph AM, Hope TJ (2006) Proteasome inhibitors uncouple rhesus TRIM5alpha restriction of HIV-1 reverse transcription and infection. Proceedings of the National Academy of Sciences of the United States of America 103: 7465–7470.
24. Anderson JL, Campbell EM, Wu X, Vandegraaff N, Engelman A, et al. (2006) Proteasome inhibition reveals that a functional preintegration complex intermediate can be generated during restriction by diverse TRIM5 proteins. Journal of Virology 80: 9754–9760.
25. Pertel T, Reinhard C, Luban J (2011) Vpx rescues HIV-1 transduction of dendritic cells from the antiviral state established by type 1 interferon. Retrovirology 8: 49.
26. Sokolskaja E, Berthoux L, Luban J (2006) Cyclophilin A and TRIM5alpha independently regulate human immunodeficiency virus type 1 infectivity in human cells. Journal of Virology 80: 2855–2862.
27. Pertel T, Hausmann S, Morger D, Zuger S, Guerra J, et al. (2011) TRIM5 is an innate immune sensor for the retrovirus capsid lattice. Nature 472: 361–365.
28. Kono K, Song H, Yokoyama M, Sato H, Shioda T, et al. (2010) Multiple sites in the N-terminal half of simian immunodeficiency virus capsid protein contribute to evasion from rhesus monkey TRIM5alpha-mediated restriction. Retrovirology 7: 72.
29. Pornillos O, Ganser-Pornillos BK, Kelly BN, Hua Y, Whitby FG, et al. (2009) X-ray structures of the hexameric building block of the HIV capsid. Cell 137: 1282–1292.
30. Ganser-Pornillos BK, Yeager M, Sundquist WI (2008) The structural biology of HIV assembly. Curr Opin Struct Biol 18: 203–217.
31. Inagaki N, Takeuchi H, Yokoyama M, Sato H, Ryo A, et al. (2010) A structural constraint for functional interaction between N-terminal and C-terminal domains in simian immunodeficiency virus capsid proteins. Retrovirology 7: 90.
32. Bailey GD, Hyun JK, Mitra AK, Kingston RL (2012) A structural model for the generation of continuous curvature on the surface of a retroviral capsid. J Mol Biol 417: 212–223.
33. Gao F, Yue L, White AT, Pappas PG, Barchue J, et al. (1992) Human infection by genetically diverse SIVSM-related HIV-2 in west Africa. Nature 358: 495–499.
34. Hillis DM, Bull JJ (1993) An empirical test of bootstrapping as a method for assessing confidence in phylogenetic analysis. Syst Biol 42: 182–192.
35. Pear WS, Nolan GP, Scott ML, Baltimore D (1993) Production of high-titer helper-free retroviruses by transient transfection. Proc Natl Acad Sci U S A 90: 8392–8396.
36. Lasfargues EY, Lasfargues JC, Dion AS, Greene AE, Moore DH (1976) Experimental infection of a cat kidney cell line with the mouse mammary tumor virus. Cancer Res 36: 67–72.
37. Sheehy AM, Gaddis NC, Choi JD, Malim MH (2002) Isolation of a human gene that inhibits HIV-1 infection and is suppressed by the viral Vif protein. Nature 418: 646–650.
38. Dodson GG, Lane DP, Verma CS (2008) Molecular simulations of protein dynamics: new windows on mechanisms in biology. EMBO Rep 9: 144–150.
39. Baker D, Sali A (2001) Protein structure prediction and structural genomics. Science 294: 93–96.
40. Shirakawa K, Takaori-Kondo A, Yokoyama M, Izumi T, Matsui M, et al. (2008) Phosphorylation of APOBEC3G by protein kinase A regulates its interaction with HIV-1 Vif. Nat Struct Mol Biol 15: 1184–1191.
41. Case DA, Darden TA, Cheatham I, T.E., Simmerling CL, Wang JR, et al. (2006) AMBER 9. University of California, San Francisco.
42. Hornak V, Abel R, Okur A, Strockbine B, Roitberg A, et al. (2006) Comparison of multiple Amber force fields and development of improved protein backbone parameters. Proteins 65: 712–725.
43. Ryckaert J-P, Ciccotti G, Berendsen HJC (1977) Numerical integration of the cartesian equations of motion of a system with constraints: Molecular dynamics of n-alkanes. J Comput Phys 23: 327–341.
44. Ponder JW, Case DA (2003) Force fields for protein simulations. Adv Protein Chem 66: 27–85.
45. Lee K, Chu CK (2001) Molecular modeling approach to understanding the mode of action of L-nucleosides as antiviral agents. Antimicrob Agents Chemother 45: 138–144.
46. Kinomoto M, Yokoyama M, Sato H, Kojima A, Kurata T, et al. (2005) Amino acid 36 in the human immunodeficiency virus type 1 gp41 ectodomain controls fusogenic activity: implications for the molecular mechanism of viral escape from a fusion inhibitor. Journal of Virology 79: 5996–6004.

frontiers in MICROBIOLOGY

ORIGINAL RESEARCH ARTICLE
published: 05 June 2012
doi: 10.3389/fmicb.2012.00206

Electrostatic potential of human immunodeficiency virus type 2 and rhesus macaque simian immunodeficiency virus capsid proteins

Katarzyna Bozek[1], Emi E. Nakayama[2], Ken Kono[2] and Tatsuo Shioda[2]*

[1] *Max Planck Institute for Informatics, Saarbrücken, Germany*
[2] *Department of Viral Infections, Research Institute for Microbial Diseases, Osaka University, Suita, Osaka, Japan*

Edited by:
Masaru Yokoyama, National Institute of Infectious Diseases, Japan

Reviewed by:
Masako Nomaguchi, The University of Tokushima Graduate School, Japan
Masaru Yokoyama, National Institute of Infectious Diseases, Japan

***Correspondence:**
Tatsuo Shioda, Department of Viral Infections, Research Institute for Microbial Diseases, Osaka University, 3-1, Yamada-oka, Suita, Osaka 565-0871, Japan.
e-mail: shioda@biken.osaka-u.ac.jp

Human immunodeficiency virus type 2 (HIV-2) and simian immunodeficiency virus isolated from a macaque monkey (SIVmac) are assumed to have originated from simian immunodeficiency virus isolated from sooty mangabey (SIVsm). Despite their close similarity in genome structure, HIV-2 and SIVmac show different sensitivities to TRIM5α, a host restriction factor against retroviruses. The replication of HIV-2 strains is potently restricted by rhesus (Rh) monkey TRIM5α, while that of SIVmac strain 239 (SIVmac239) is not. Viral capsid protein is the determinant of this differential sensitivity to TRIM5α, as the HIV-2 mutant carrying SIVmac239 capsid protein evaded Rh TRIM5α-mediated restriction. However, the molecular determinants of this restriction mechanism are unknown. Electrostatic potential on the protein-binding site is one of the properties regulating protein–protein interactions. In this study, we investigated the electrostatic potential on the interaction surface of capsid protein of HIV-2 strain GH123 and SIVmac239. Although HIV-2 GH123 and SIVmac239 capsid proteins share more than 87% amino acid identity, we observed a large difference between the two molecules with the HIV-2 GH123 molecule having predominantly positive and SIVmac239 predominantly negative electrostatic potential on the surface of the loop between α-helices 4 and 5 (L4/5). As L4/5 is one of the major determinants of Rh TRIM5α sensitivity of these viruses, the present results suggest that the binding site of the Rh TRIM5α may show complementarity to the HIV-2 GH123 capsid surface charge distribution.

Keywords: HIV-2, SIVmac, capsid, TRIM5α, electrostatic potential, APBS, SAS

INTRODUCTION

The host range of human immunodeficiency virus type 1 (HIV-1) is narrow, limited to humans and chimpanzees (Gao et al., 1999). HIV-1 fails to replicate in activated CD4-positive T lymphocytes from Old World monkeys (OWM), such as rhesus (Rh; Shibata et al., 1995; Himathongkham and Luciw, 1996) and cynomolgus (CM) monkeys (Akari et al., 1996, 1999). On the other hand, simian immunodeficiency virus (SIV) isolated from sooty mangabey (SIVsm) and SIV isolated from African green monkey (SIVagm) replicate well in their natural hosts (VandeWoude and Apetrei, 2006). SIV isolated from a macaque monkey (SIVmac) evolved from SIVsm in captive macaques, and replicates efficiently in Rh (Shibata et al., 1995; Himathongkham and Luciw, 1996) and CM (Akari et al., 1996, 1999) monkeys. Human immunodeficiency virus type 2 (HIV-2) is assumed to have originated from SIVsm as the result of zoonotic events involving monkeys and humans (Hahn et al., 2000). Previous studies have shown that HIV-2 strains vary widely in their ability to grow in cells of OWM (Castro et al., 1990, 1991; Locher et al., 1998, 2003; Fujita et al., 2003).

TRIM5α was identified as an anti-HIV-1 host restriction factor in Rh monkey cells (Stremlau et al., 2004). TRIM5 proteins are members of the tripartite motif family containing RING, B-box, and coiled-coil domains. The α isoform of TRIM5 has an additional C-terminal PRYSPRY domain (Reymond et al., 2001). TRIM5α recognizes the multimerized capsid (viral core) of an incoming virus by its PRYSPRY domain and causes degradation of the core (Sebastian and Luban, 2005; Stremlau et al., 2006). In CM monkey, TRIM5α has also been shown to restrict HIV-1 infection (Nakayama et al., 2005).

We previously evaluated the sensitivity of HIV-2 and SIVmac to Rh and CM TRIM5αs, and found that HIV-2 strain GH123 carrying P at position 120 of the capsid protein (CA) was potently restricted by CM TRIM5α, while the HIV-2 GH123 mutant in which P was replaced with Q was resistant to CM TRIM5α (Song et al., 2007). In contrast, Rh TRIM5α potently restricted the replication of both viruses (Kono et al., 2008). Three amino acid residues, TFP, at positions 339–341 in the PRYSPRY domain of Rh TRIM5α were necessary for restricting HIV-2 strains that were resistant to CM TRIM5α (Kono et al., 2008). Although SIVmac239 CA possesses Q at position 118 corresponding to position 120 of GH123, SIVmac239 was resistant to both of CM and Rh TRIM5αs (Kono et al., 2008, 2010). Therefore, we attempted to identify the viral determinant of SIVmac239 underlying evasion from Rh TRIM5α-mediated restriction, and found that multiple regions including the N-terminal loop, a loop between α-helices 4 and 5 (L4/5), and a loop between α-helices 6 and 7 (L6/7) in

the N-terminal half of SIVmac239 CA are necessary for complete evasion of Rh TRIM5α restriction (Kono et al., 2010).

Apart from the sequence and structural characteristics regulating protein–protein interaction, the electrostatic potential at the binding site is an important factor allowing molecular interactions. The electrostatic potential on the protein surface is generated through redistribution of electrons according to local electrical fields. It is defined as the potential energy of a proton at a particular location near a molecule. Negative electrostatic potential results in attraction of the proton by the concentrated electron density. Positive electrostatic potential results in repulsion of the proton by the atomic nuclei in regions where low electron density exists and nuclear charge is incompletely shielded. Electrostatic effects were shown to be a major factor in determining the nature and strength of the interactions between protein surfaces (Dong and Zhou, 2002; Kortemme and Baker, 2002). A complementary charge on the binding site of both proteins may result in an attractive force allowing binding to occur.

In the present study, we analyzed the electrostatic potentials of the surface regions of the CA loop. We analyzed two CA variants, HIV-2 GH123 and SIVmac239 CAs, showing opposite restriction phenotypes. We first modeled the 3-D structures of the proteins by homology modeling and next calculated the electrostatic potentials in the regions of interest based on Adaptive Poisson–Boltzmann Solver and non-local electrostatic method. We found a large difference in the electrostatic potentials of the loop surface between the HIV-2 GH123 and SIVmac239 CAs, potentially responsible for the differential TRIM5α sensitivity of these two viruses.

MATERIALS AND METHODS

MODELING

The structure of the N-terminal domain of the HIV-1 CA (PDB number 1GWP; Tang et al., 2002) was used as a template for building the corresponding domain models of HIV-2 GH123 and SIVmac239 CAs. The models were built using Modeller 9v4 (Eswar et al., 2007) and visualized with PyMOL (http://www.pymol.org).

CALCULATION OF ELECTROSTATIC POTENTIALS

As the initial step preceding electrostatic potential modeling, we added missing hydrogen atoms and estimated the ionization (protonation) of the molecules. We used H++ server (Gordon et al., 2005) http://biophysics.cs.vt.edu/H++, which adds protons to the input structure according to the calculated ionization states at the specified pH of the solvent. The H++ method models molecules as a low dielectric medium ε_{in} in a solvent with a high dielectric constant ε_{out}. It additionally allows the user to define the salt concentration of the medium and its pH. We used the most biologically relevant parameters of human cells: pH = 7.2, salinity 1%, molecule dielectric $\varepsilon_{in} = 10$, and medium dielectric $\varepsilon_{in} = 80$. The dielectric parameters were chosen according to the suggestions of the authors of the H++ method as appropriate for modeling protonation of surface residues. We also inspected electrostatic potential profiles resulting from several other parameter combinations. Other parameter regimes did not produce markedly different electrostatic potentials in the region of interest. Therefore, we chose the initial parameters as the most relevant for biological settings.

We next applied two methods of electrostatic potential calculation: Adaptive Poisson–Boltzmann Solver (APBS; Baker et al., 2001) and non-local electrostatic method (Hildebrandt et al., 2007). In both methods, electrostatic properties are described by the Poisson–Boltzmann equation, a second-order non-linear partial differential equation. APBS method solves the equation using finite element techniques based on parameter discretization and iterative parallel refinement of the equation solution. The non-local electrostatic method allows inclusion of the structure of water molecules in the calculation and describes the system as a continuum. This method captures the effects of the dipole polarization of water molecules and the effects of the surrounding hydrogen bond network, and is therefore a more accurate model of the electrostatic potential estimations close to the molecule-solvent interface.

We used two different surface approximations: solvent-accessible surface (SAS) of two different sizes. SAS is the surface of a molecule that is accessible to a solvent. It is estimated using a "rolling ball" approach (Shrake and Rupley, 1973) in which a sphere of solvent of a particular radius is used to probe the surface of the molecule, the surface is then described by the center of the probing sphere. We used the approximate radius of a water molecule of 1.4 Å and an additional 3 Å to determine how the electrostatic potential changes with distance from the molecule.

RESULTS

THE 3-D STRUCTURAL MODELS OF HIV-2 GH123 AND SIVmac239 CA N-TERMINAL DOMAINS

Previously, we evaluated the sensitivity of HIV-2 GH123 and SIVmac239 to Rh and CM TRIM5αs, and found that HIV-2 GH123 was sensitive to CM and Rh TRIM5αs (Song et al., 2007; Kono et al., 2008; **Figure 1A**). In contrast, SIVmac239 was resistant to CM and Rh TRIM5αs (Kono et al., 2008, 2010; **Figure 1A**). CA is the determinant for this differential sensitivity to TRIM5α between HIV-2 GH123 and SIVmac239, as the HIV-2 GH123 mutant carrying SIVmac239 CA (HIV-2 GH/SCA) was also resistant to CM and Rh TRIM5αs (**Figure 1A**; Kono et al., 2010). Despite this marked difference in TRIM5α sensitivity between HIV-2 GH123 and SIVmac239, CA of these two viruses share more than 87% amino acid identity (**Figure 1B**). Therefore, we compared the structural properties of HIV-2 GH123 CA with those of SIVmac239.

We first constructed 3-D models of HIV-2 GH123 and SIVmac239 CA N-terminal domains by homology modeling. In the constructed models, HIV-2 GH123 and SIVmac239 CA N-terminal domains showed the most striking differences in shape of surface exposed loops (**Figure 2**). SIVmac239 CA is characterized by a more contracted shape as compared to the expanded loop structure of HIV-2 GH123. To confirm that this shape difference is not due to modeling noise, we remodeled both proteins using each one as a template for the other. The remodeled structures showed similar shape differences (data not shown), suggesting that the real structures differ.

ELECTROSTATIC POTENTIALS OF HIV-2 GH123 AND SIVmac239 CA N-TERMINAL DOMAINS

Figure 3 shows the distributions of calculated electrostatic potentials of HIV-2 GH123 and SIVmac239 CA N-terminal domains. We observed strong differences between the two molecules on

A

	CM TRIM5α	Rh TRIM5α
HIV-2 GH123	Sensitive	Sensitive
HIV-2 GH/SCA	Resistant	Resistant
SIVmac239	Resistant	Resistant

B

N-terminal

```
HIV-2 GH123   1 PVQQTGGGNYIHVPLSPRTLNAWVKLVEDKKFGAEVVPGFQALSEGCTPYDINQMLNCVG   60
SIVmac239     1 ....I..-..V.L.............I.E.............................   59

                                                  L4/5
HIV-2 GH123  61 DHQAAMQIIREIINDEAADWDAQHPIPGPLPAGQLRDPRGSDIAGTTSTVEEQIQWMYRP  120
SIVmac239    60 ..........D...E......L...Q.A.-QQ....E.S.........S.D........Q  118

             L6/7
HIV-2 GH123 121 QNPVPVGNIYRRWIQIGLQKCVRMYNPTNILDVKQGPKEPFQSYVDRFYKSLRAEQTDPA  180
SIVmac239   119 ..I..........L.............................................A.  178


HIV-2 GH123 181 VKNWMTQTLLIQNANPDCKLVLKGLGMNPTLEEMLTACQGVGGPGQKARLM          231
SIVmac239   179 ........................V.........................          229
```

FIGURE 1 | (A) Sensitivities of HIV-2 GH123, HIV-2 GH123 mutant carrying SIVmac239 capsid protein (HIV-2 GH/SCA), and SIVmac239 to cynomolgus (CM) and rhesus (Rh) monkey TRIM5α. The replication of HIV-2 GH123 was potently restricted by CM and Rh TRIM5α (sensitive), while that of SIVmac239 and the HIV-2 GH123 mutant carrying SIVmac239 capsid was not (resistant). **(B)** Alignment of amino acid sequences of HIV-2 GH123 and SIVmac239 capsid proteins. Positions of the N-terminal loop (N-terminal), a loop between α-helices 4 and 5 (L4/5), and a loop between α-helices 6 and 7 (L6/7) are indicated above the amino acid sequences.

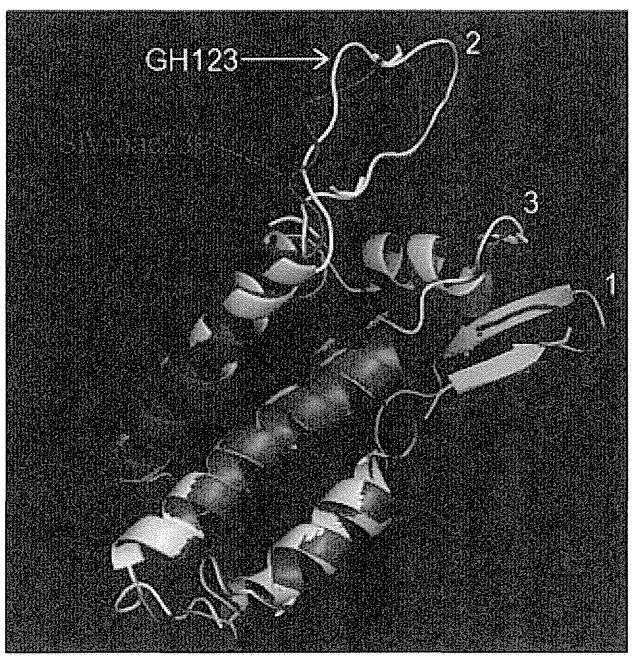

FIGURE 2 | Superposition of modeled structures of the N-terminal domains of HIV-2 GH123 (GH123, yellow) and SIVmac239 (red) capsid proteins. The three loops containing sites important for the TRIM5α interaction are numbered as follows: (1) N-terminal loop, (2) loop between α-helices 4 and 5 (L4/5), (3) loop between α-helices 6 and 7 (L6/7).

the surface of the loops with the GH123 molecule having predominantly positive and SIVmac239 predominantly negative electrostatic potential on this part of the surface (**Figure 3**).

To quantify this observation and obtain further insight into the specific region where the electrostatic potential differences are strong, we extracted the electrostatic potential values on the surfaces of the two molecules. From the electrostatic potential values estimated in a grid covering the entire space around the molecules, we extracted grid points neighboring the points of triangulation of each surface type. We grouped these electrostatic potential values according to the atoms of the closest loop residues. This comparison of grouped electrostatic potential values of corresponding residues in the two analyzed molecules allowed us to quantitatively confirm the differences in electrostatic potential in the region of interest and to point to specific residues around which the differences were stronger. The strongest difference in electrostatic potential between HIV-2 GH123 and SIVmac239 CAs was observed on the surface of L4/5, with HIV-2 GH123 and SIVmac239 showing positive and negative electrostatic potential, respectively. Eight of nine residues in this loop showed significant differences in mean electrostatic potential and clear separation of the electrostatic potential values on the grid neighboring to the loop residues by both local ABPS and non-local electrostatic methods (**Table 1**).

Residues in L6/7 showed weak but similar electrostatic potential differences to those of L4/5 by the local ABPS method, but these differences were not confirmed by the non-local electrostatic method (**Table 1**). The N-terminal loop showed the opposite pattern, with HIV-2 GH123 and SIVmac239 having negative and positive electrostatic potentials, respectively, according to the local APBS method (**Table 1**). However, the differences were smaller and were not confirmed by the non-local electrostatic method (**Table 1**).

Similar electrostatic potential differences, although spanning a narrower range of values than those described above, were

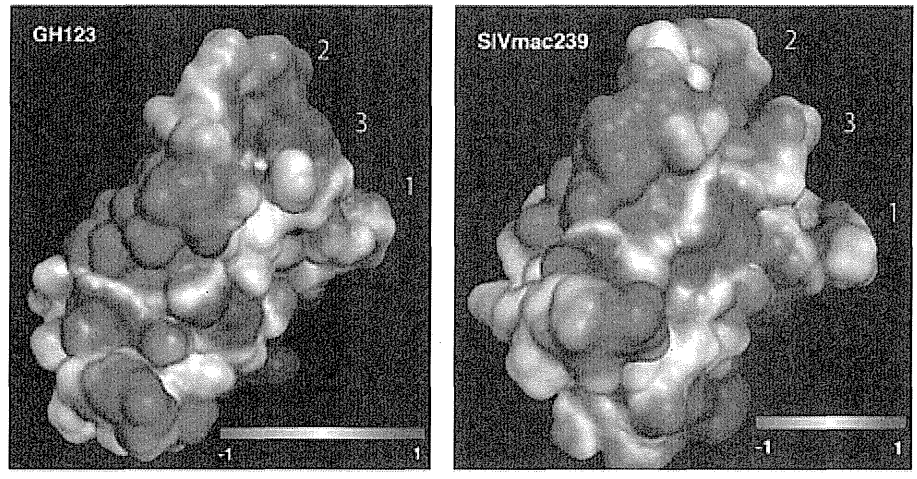

FIGURE 3 | Electrostatic potential on the surface of HIV-2 GH123 (GH123) and SIVmac239 capsid protein N-terminal domains. Structures are positioned as in **Figure 2** with the loops directed toward the upper right of the image. Electrostatic potential was calculated and visualized using the APBS plugin in PyMOL. The three loops containing sites important for the TRIM5α interaction are numbered as follows: (1) N-terminal loop, (2) loop between α-helices 4 and 5 (L4/5), (3) loop between α-helices 6 and 7 (L6/7).

Table 1 | Mean electrostatic potential on the surface surrounding residues of the N-terminal loop (N-terminal), the loop between α-helices 4 and 5 (L4/5), and the loop between α-helices 6 and 7 (L6/7) of HIV-2 GH123 and SIVmac239 CAs calculated using the local Adaptive Poisson–Boltzmann Solver (APBS) and non-local electrostatic methods.

	Residue (GH123/SIVmac239)	APBS			Non-local		
		HIV-2 GH123	SIVmac239	*p*-Value	HIV-2 GH123	SIVmac239	*p*-Value
N-terminal	5 THR/5 ILE	−0.206	0.064	<0.001	−1.049	−0.096	<0.001
	6 GLY/6 GLY	0.025	−0.196	0.006	0.787	−0.805	<0.001
	7 GLY/7 GLY	−0.315	0.024	<0.001	−1.283	−0.854	<0.001
	8 GLY/8 ASN	−0.420	0.066	<0.001	0.058	−1.092	0.406
	9 ASN/9 TYR	−0.463	−0.241	0.741	−5.668	2.697	<0.001
	10 TYR/10 VAL	−0.782	0.021	<0.001	−8.827	−1.367	<0.001
L4/5	88 GLY/87 ALA	0.147	−0.248	<0.001	2.906	−1.700	<0.001
	89 PRO/88 PRO	0.355	−0.522	<0.001	2.879	−0.524	<0.001
	90 LEU/–	−0.426	–	–	6.567	–	–
	91 PRO/89 GLN	0.603	−0.133	<0.001	6.543	−0.673	<0.001
	92 ALA/90 GLN	0.047	−0.051	<0.001	1.282	−0.418	<0.001
	93 GLY/91 GLY	−0.230	−0.269	0.076	−2.761	3.070	<0.001
	94 GLN/92 GLN	0.895	−0.735	<0.001	7.148	0.820	<0.001
	95 LEU/93 LEU	−0.958	−1.433	0.046	−6.661	2.234	<0.001
	96 ARG/94 ARG	0.090	−0.227	<0.001	5.805	−3.992	<0.001
	97 ASP/95 GLU	−0.045	−1.599	<0.001	−8.336	−3.481	0.001
L6/7	117 MET/115 MET	−0.765	0.799	<0.001	−6.437	−9.665	0.078
	118 TYR/116 TYR	0.070	−0.069	0.167	−5.037	0.055	<0.001
	119 ARG/117 ARG	1.022	0.405	<0.001	6.785	−2.802	<0.001
	120 PRO/118 GLN	−0.094	−0.706	<0.001	−5.178	3.904	<0.001
	121 GLN/119 GLN	0.802	−0.260	<0.001	4.308	0.340	<0.001
	122 ASN/120 ASN	0.119	−0.674	<0.001	−4.078	−6.824	0.003
	123 PRO/121 PRO	−0.782	−0.235	<0.001	−17.281	−11.590	<0.001
	124 VAL/122 ILE	−1.200	−1.906	<0.001	−6.233	−8.141	0.003
	125 PRO/123 PRO	−0.250	0.455	<0.001	−4.804	−12.468	<0.001

Color indicates significant difference ($p < 0.05$, Wilcoxon test) between the electrostatic potentials of the two molecules with positive electrostatic potential marked in blue and negative marked in red.

observed on the SAS of the 3 Å probe radius (data not shown). These observations reflect the electrostatic potential decrease with distance from the molecule surface.

DISCUSSION

In the present study, we constructed 3-D models of HIV-2 GH123 and SIVmac239 CA N-terminal domains by homology modeling and analyzed the electrostatic potential distributions on the SASs of these molecules. We observed a large difference between the HIV-2 GH123 and SIVmac239 CA N-terminal domains, with the HIV-2 GH123 molecule having predominantly positive and SIVmac239 predominantly negative electrostatic potential on the surface of L4/5. This result may be relevant to the previous findings that CA L4/5 was one of the major determinants for the differential sensitivity to Rh TRIM5α between HIV-2 and SIVmac239 (Ylinen et al., 2005; Kono et al., 2010).

Precise calculation of the interaction electrostatics is challenging due to the large surfaces involved and the large structural changes that can occur upon binding. Here, our quantitative approach based on two different methods for calculation of electrostatic potential indicated negative electrostatic potential on the surface of the resistant CA variant SIVmac239 and positive electrostatic potential of the non-resistant HIV-2 GH123 variant. The presence of positive electrostatic potential on the surface of L4/5 may therefore be a prerequisite for the interactions with Rh TRIM5α. This loop is the most outward pointing part of the CA protein. Complementarity to the HIV-2 GH123 surface charge distribution at the binding site of the host protein may be necessary for binding. Therefore, similar studies of TRIM5α surface electrostatic potentials could help to point to the specific site of this interaction, although the 3-D structural analysis of TRIM5α PRYSPRY domain is required for this goal.

It was recently reported that a recombinant TRIM5α protein carrying TRIM21 RING domain (TRIM5-21R) assembled to form 2-D paracrystalline hexagonal arrays *in vitro* (Ganser-Pornillos et al., 2011). This assembly requires RING and B-box 2 domains, and the hexagonal lattices of HIV-1 CA that mimic the surface of core act as template for stabilization of TRIM5-21R arrays in a PRYSPRY-dependent manner (Ganser-Pornillos et al., 2011). As the interaction between individual CA monomers and TRIM5α is very weak, CA recognition by TRIM5α is thought to be a synergistic combination of direct binding interactions with the PRYSPRY domain, higher-order assembly of TRIM5α, template-based assembly, and lattice complementarity. Therefore, the electrostatic potential might be the crucial determinant of this binding allowing TRIM5α for recognition of a broader range of CA sequence variants.

In addition to L4/5, our previous study revealed that the N-terminal loop and L6/7 in the N-terminal half of SIVmac239 CA are also necessary for complete evasion of Rh TRIM5α restriction (Kono et al., 2010). Electrostatic potentials of these 2 loops did not show large differences between HIV-2 GH123 and SIVmac239. Therefore, it is possible that a certain interaction other than the electrostatic interaction would be involved in binding of Rh TRIM5α PRYSPRY domain with the N-terminal loop and L6/7 of HIV-2 GH123.

On sodium dodecyl sulfate (SDS)-polyacrylamide gel electrophoresis, SIVmac239 CA is known to migrate at a molecular weight of 27 kDa, while HIV-2 GH123 CA migrates at a molecular weight of 25 kDa (Kono et al., 2010). However, the number of amino acid residues in SIVmac239 CA is smaller than that in HIV-2 GH123 CA (**Figure 1B**), and the molecular weight of SIVmac239 CA is therefore smaller than that of HIV-2 GH123. We reported previously that the amino acid sequences of L4/5 determined this differential electrophoretic mobility of CAs (Kono et al., 2010). The difference seems to be attributable to the presence of non-polar P and A residues at positions 91 and 92, respectively, in L4/5 of HIV-2 GH123 CA, where two more hydrophilic Q residues are located in SIVmac239 CA L4/5 (**Figure 1**; **Table 1**). In addition, HIV-2 GH123 CA L4/5 has a hydrophobic L insertion at position 90 (**Figure 1**; **Table 1**). Therefore, L4/5 of HIV-2 GH123 CA is more hydrophobic and would attract larger numbers of SDS molecules than that of SIVmac239 leading to accelerated electrophoretic speed of the CA. It is therefore possible that hydrophobic interactions between Rh TRIM5α and viral CAs would also be involved in determining the anti-viral specificity of TRIM5α in addition to the electrostatic interactions discussed above. Further biochemical studies of TRIM5α and viral CAs are necessary to address this question.

ACKNOWLEDGMENTS

We thank Dr. Thomas Lengauer for his support and Ms. Noriko Teramoto for her help. This work was supported by grants from the Ministry of Education, Culture, Sports, Science, and Technology, and the Ministry of Health, Labour and Welfare, Japan.

REFERENCES

Akari, H., Mori, K., Terao, K., Otani, I., Fukasawa, M., Mukai, R., and Yoshikawa, Y. (1996). In vitro immortalization of old world monkey T lymphocytes with *Herpesvirus saimiri*: its susceptibility to infection with simian immunodeficiency viruses. *Virology* 218, 382–388.

Akari, H., Nam, K. H., Mori, K., Otani, I., Shibata, H., Adachi, A., Terao, K., and Yoshikawa, Y. (1999). Effects of SIVmac infection on peripheral blood CD4+CD8+ T lymphocytes in *Cynomolgus macaques*. *Clin. Immunol.* 91, 321–329.

Baker, N. A., Sept, D., Joseph, S., Holst, M. J., and McCammon, J. A. (2001). Electrostatics of nanosystems: application to microtubules and the ribosome. *Proc. Natl. Acad. Sci. U.S.A.* 98, 10037–10041.

Castro, B. A., Barnett, S. W., Evans, L. A., Moreau, J., Odehouri, K., and Levy, J. A. (1990). Biologic heterogeneity of human immunodeficiency virus type 2 (HIV-2) strains. *Virology* 178, 527–534.

Castro, B. A., Nepomuceno, M., Lerche, N. W., Eichberg, J. W., and Levy, J. A. (1991). Persistent infection of baboons and rhesus monkeys with different strains of HIV-2. *Virology* 184, 219–226.

Dong, F., and Zhou, H. X. (2002). Electrostatic contributions to T4 lysozyme stability: solvent-exposed charges versus semi-buried salt bridges. *Biophys. J.* 83, 1341–1347.

Eswar, N., Webb, B., Marti-Renom, M. A., Madhusudhan, M. S., Eramian, D., Shen, M. Y., Pieper, U., and Sali, A. (2007). Comparative protein structure modeling using MODELLER. *Curr. Protoc. Protein Sci.* Chap. 2, Unit 2.9.

Fujita, M., Yoshida, A., Sakurai, A., Tatsuki, J., Ueno, F., Akari, H., and Adachi, A. (2003). Susceptibility of HVS-immortalized lymphocytic HSC-F cells to various strains and mutants of HIV/SIV. *Int. J. Mol. Med.* 11, 641–644.

Ganser-Pornillos, B. K., Chandrasekaran, V., Pornillos, O., Sodroski, J. G., Sundquist, W. I., and Yeager, M. (2011). Hexagonal assembly of a restricting TRIM5alpha protein. *Proc. Natl. Acad. Sci. U.S.A.* 108, 534–539.

Gao, F., Bailes, E., Robertson, D. L., Chen, Y., Rodenburg, C. M., Michael, S. F., Cummins, L. B., Arthur, L. O., Peeters, M., Shaw, G. M., Sharp, P. M., and Hahn, B. H. (1999). Origin of HIV-1 in the chimpanzee Pan troglodytes troglodytes. *Nature* 397, 436–441.

Gordon, J. C., Myers, J. B., Folta, T., Shoja, V., Heath, L. S., and Onufriev, A. (2005). H++: a server for estimating pKas and adding missing hydrogens to macromolecules. *Nucleic Acids Res.* 33, W368–W371.

Hahn, B. H., Shaw, G. M., De Cock, K. M., and Sharp, P. M. (2000). AIDS as a zoonosis: scientific and public health implications. *Science* 287, 607–614.

Hildebrandt, A., Blossey, R., Rjasanow, S., Kohlbacher, O., and Lenhof, H. P. (2007). Electrostatic potentials of proteins in water: a structured continuum approach. *Bioinformatics* 23, e99–e103.

Himathongkham, S., and Luciw, P. A. (1996). Restriction of HIV-1 (subtype B) replication at the entry step in rhesus macaque cells. *Virology* 219, 485–488.

Kono, K., Song, H., Shingai, Y., Shioda, T., and Nakayama, E. E. (2008). Comparison of anti-viral activity of rhesus monkey and cynomolgus monkey TRIM5alphas against human immunodeficiency virus type 2 infection. *Virology* 373, 447–456.

Kono, K., Song, H., Yokoyama, M., Sato, H., Shioda, T., and Nakayama, E. E. (2010). Multiple sites in the N-terminal half of simian immunodeficiency virus capsid protein contribute to evasion from rhesus monkey TRIM5alpha-mediated restriction. *Retrovirology* 7, 72.

Kortemme, T., and Baker, D. (2002). A simple physical model for binding energy hot spots in protein-protein complexes. *Proc. Natl. Acad. Sci. U.S.A.* 99, 14116–14121.

Locher, C. P., Blackbourn, D. J., Herndier, B. G., Reyes-Teran, G., Barnett, S. W., Murthy, K. K., and Levy, J. A. (1998). Transient virus infection and pathogenesis of a new HIV type 2 isolate, UC12, in baboons. *AIDS Res. Hum. Retroviruses* 14, 79–82.

Locher, C. P., Witt, S. A., Herndier, B. G., Abbey, N. W., Tenner-Racz, K., Racz, P., Kiviat, N. B., Murthy, K. K., Brasky, K., Leland, M., and Levy, J. A. (2003). Increased virus replication and virulence after serial passage of human immunodeficiency virus type 2 in baboons. *J. Virol.* 77, 77–83.

Nakayama, E. E., Miyoshi, H., Nagai, Y., and Shioda, T. (2005). A specific region of 37 amino acid residues in the SPRY (B30.2) domain of African green monkey TRIM5 alpha determines species-specific restriction of simian immunodeficiency virus SIVmac infection. *J. Virol.* 79, 8870–8877.

Reymond, A., Meroni, G., Fantozzi, A., Merla, G., Cairo, S., Luzi, L., Riganelli, D., Zanaria, E., Messali, S., Cainarca, S., Guffanti, A., Minucci, S., Pelicci, P. G., and Ballabio, A. (2001). The tripartite motif family identifies cell compartments. *EMBO J.* 20, 2140–2151.

Sebastian, S., and Luban, J. (2005). TRIM5alpha selectively binds a restriction-sensitive retroviral capsid. *Retrovirology* 2, 40.

Shibata, R., Sakai, H., Kawamura, M., Tokunaga, K., and Adachi, A. (1995). Early replication block of human immunodeficiency virus type 1 in monkey cells. *J. Gen. Virol.* 76(Pt 11), 2723–2730.

Shrake, A., and Rupley, J. A. (1973). Environment and exposure to solvent of protein atoms. Lysozyme and insulin. *J. Mol. Biol.* 79, 351–371.

Song, H., Nakayama, E. E., Yokoyama, M., Sato, H., Levy, J. A., and Shioda, T. (2007). A single amino acid of the human immunodeficiency virus type 2 capsid affects its replication in the presence of cynomolgus monkey and human TRIM5alphas. *J. Virol.* 81, 7280–7285.

Stremlau, M., Owens, C. M., Perron, M. J., Kiessling, M., Autissier, P., and Sodroski, J. (2004). The cytoplasmic body component TRIM5alpha restricts HIV-1 infection in old world monkeys. *Nature* 427, 848–853.

Stremlau, M., Perron, M., Lee, M., Li, Y., Song, B., Javanbakht, H., Diaz-Griffero, F., Anderson, D. J., Sundquist, W. I., and Sodroski, J. (2006). Specific recognition and accelerated uncoating of retroviral capsids by the TRIM5alpha restriction factor. *Proc. Natl. Acad. Sci. U.S.A.* 103, 5514–5519.

Tang, C., Ndassa, Y., and Summers, M. F. (2002). Structure of the N-terminal 283-residue fragment of the immature HIV-1 Gag polyprotein. *Nat. Struct. Biol.* 9, 537–543.

VandeWoude, S., and Apetrei, C. (2006). Going wild: lessons from naturally occurring T-lymphotropic lentiviruses. *Clin. Microbiol. Rev.* 19, 728–762.

Ylinen, L. M., Keckesova, Z., Wilson, S. J., Ranasinghe, S., and Towers, G. J. (2005). Differential restriction of human immunodeficiency virus type 2 and simian immunodeficiency virus SIVmac by TRIM5 alpha alleles. *J. Virol.* 79, 11580–11587.

Conflict of Interest Statement: The authors declare that the research was conducted in the absence of any commercial or financial relationships that could be construed as a potential conflict of interest.

Received: 19 April 2012; paper pending published: 18 May 2012; accepted: 21 May 2012; published online: 05 June 2012.

Citation: Bozek K, Nakayama EE, Kono K and Shioda T (2012) Electrostatic potential of human immunodeficiency virus type 2 and rhesus macaque simian immunodeficiency virus capsid proteins. Front. Microbio. 3:206. doi: 10.3389/fmicb.2012.00206

This article was submitted to Frontiers in Virology, a specialty of Frontiers in Microbiology.

JVI Journals.ASM.org

Association of Major Histocompatibility Complex Class I Haplotypes with Disease Progression after Simian Immunodeficiency Virus Challenge in Burmese Rhesus Macaques

Takushi Nomura,[a,b] Hiroyuki Yamamoto,[a] Teiichiro Shiino,[a] Naofumi Takahashi,[a,b] Taku Nakane,[a,b] Nami Iwamoto,[a,b] Hiroshi Ishii,[a,b] Tetsuo Tsukamoto,[b] Miki Kawada,[b] Saori Matsuoka,[a] Akiko Takeda,[a] Kazutaka Terahara,[c] Yasuko Tsunetsugu-Yokota,[c] Naoko Iwata-Yoshikawa,[d] Hideki Hasegawa,[d] Tetsutaro Sata,[d] Taeko K. Naruse,[e] Akinori Kimura,[e] and Tetsuro Matano[a,b]

AIDS Research Center, National Institute of Infectious Diseases, Toyama, Shinjuku-ku, Tokyo, Japan[a]; The Institute of Medical Science, The University of Tokyo, Shirokanedai, Minato-ku, Tokyo, Japan[b]; Department of Immunology, National Institute of Infectious Diseases, Toyama, Shinjuku-ku, Tokyo, Japan[c]; Department of Pathology, National Institute of Infectious Diseases, Toyama, Shinjuku-ku, Tokyo, Japan[d]; and Department of Molecular Pathogenesis, Medical Research Institute, Tokyo Medical and Dental University, Kandasurugadai, Chiyoda-ku, Tokyo, Japan[e]

Nonhuman primate AIDS models are essential for the analysis of AIDS pathogenesis and the evaluation of vaccine efficacy. Multiple studies on human immunodeficiency virus and simian immunodeficiency virus (SIV) infection have indicated the association of major histocompatibility complex class I (MHC-I) genotypes with rapid or slow AIDS progression. The accumulation of macaque groups that share not only a single MHC-I allele but also an MHC-I haplotype consisting of multiple polymorphic MHC-I loci would greatly contribute to the progress of AIDS research. Here, we investigated SIVmac239 infections in four groups of Burmese rhesus macaques sharing individual MHC-I haplotypes, referred to as A, E, B, and J. Out of 20 macaques belonging to A^+ ($n = 6$), E^+ ($n = 6$), B^+ ($n = 4$), and J^+ ($n = 4$) groups, 18 showed persistent viremia. Fifteen of them developed AIDS in 0.5 to 4 years, with the remaining three at 1 or 2 years under observation. A^+ animals, including two controllers, showed slower disease progression, whereas J^+ animals exhibited rapid progression. E^+ and B^+ animals showed intermediate plasma viral loads and survival periods. Gag-specific $CD8^+$ T-cell responses were efficiently induced in A^+ animals, while Nef-specific $CD8^+$ T-cell responses were in A^+, E^+, and B^+ animals. Multiple comparisons among these groups revealed significant differences in survival periods, peripheral $CD4^+$ T-cell decline, and SIV-specific $CD4^+$ T-cell polyfunctionality in the chronic phase. This study indicates the association of MHC-I haplotypes with AIDS progression and presents an AIDS model facilitating the analysis of virus-host immune interaction.

Virus-specific $CD8^+$ cytotoxic T lymphocytes (CTLs) are major effectors against persistent virus infections (13, 44). In virus-infected cells, viral antigen-derived peptides (epitopes) are bound to major histocompatibility complex class I (MHC-I) molecules and presented on the cell surface. Viral peptide-specific CTLs recognize the peptide-MHC-I complexes by their T-cell receptors. CTL effectors deliver cell death via apoptosis as well as lysis (15, 48).

Human immunodeficiency virus type 1 (HIV-1) infection induces persistent viral replication leading to AIDS progression. CTL responses play a central role in the suppression of HIV-1 replication (6, 18, 25, 32, 43). Multiple studies on HIV-1-infected individuals have shown an association of HLA genotypes with rapid or delayed AIDS progression (14, 23, 27, 51, 54). For instance, HIV-1-infected individuals possessing *HLA-B*57* tend to show a better prognosis with lower viral loads, implicating HLA-B*57-restricted epitope-specific CTL responses in this viral control (3, 33, 34). In contrast, the association of *HLA-B*35* with rapid disease progression has been indicated (8).

Nonhuman primate AIDS models are important for the analysis of AIDS pathogenesis and the evaluation of vaccine efficacy (5, 35, 47). Models of simian immunodeficiency virus (SIV) infection in macaques are widely used currently (12, 22). Indian rhesus macaques possessing certain MHC-I alleles, such as *Mamu-A*01*, *Mamu-B*08*, and *Mamu-B*17*, tend to show lower set point plasma viral loads in SIV infection (30, 36, 37, 59). Regarding MHC-I alleles, humans have a single polymorphic HLA-A, HLA-B, and HLA-C locus per chromosome, whereas MHC-I haplotypes in macaques have variable numbers of expressed polymorphic MHC-I loci (7, 9, 26, 41). Thus, the accumulation of multiple macaque groups, each sharing a different MHC-I haplotype, would contribute to the precise analysis of SIV infection.

We have been working on the establishment of an AIDS model using Burmese rhesus macaques sharing MHC-I haplotypes (38, 50). In the present study, we have focused on SIV infection in four groups of Burmese rhesus macaques, each consisting of four or more animals. These groups share MHC-I haplotypes *90-120-Ia* (referred to as A), *90-010-Ie* (E), *90-120-Ib* (B), and *90-088-Ij* (J), respectively. The analysis of SIVmac239 infection among these groups revealed differences in plasma viral loads, peripheral $CD4^+$ T cell counts, survival periods, virus-specific CTL responses, and T-cell polyfunctionality. Our results indicate the association of MHC-I haplotypes with disease progression in SIV infection and present a sophisticated model of SIV infection.

Received 11 December 2011 Accepted 27 March 2012
Published ahead of print 4 April 2012
Address correspondence to Tetsuro Matano, tmatano@nih.go.jp.

doi:10.1128/JVI.07077-11

TABLE 1 MHC-I haplotypes

MHC-I haplotype	Confirmed MHC-I allele(s)	
	Mamu-A	*Mamu-B*
A (*90-120-Ia*)	*A1*043:01, A1*065:01*	*B*061:03, B*068:04, B*089:01*
E (*90-010-Ie*)	*A1*066:01*	*B*005:02, B*015:04*
B (*90-120-Ib*)	*A1*018:08, A2*005:31*	*B*036:03, B*037:01, B*043:01, B*162:01*
J (*90-088-Ij*)	*A1*008:01*	*B*007:02, B*039:01*

MATERIALS AND METHODS

Animal experiments. We examined SIV infections in four groups of Burmese rhesus macaques having MHC-I haplotypes *90-120-Ia* (A) ($n = 6$), *90-010-Ie* (E) ($n = 6$), *90-120-Ib* (B) ($n = 4$), and *90-088-Ij* (J) ($n = 4$). Macaques R02-007, R06-037, R07-001, R07-004, R07-009, R01-011, R06-038, R06-001, R02-004, R04-014, and R06-022, which were used as controls in previous experiments (49, 53, 58), were included in the present study. The determination of MHC-I haplotypes was based on the family study in combination with the reference strand-mediated conformation analysis (RSCA) of *Mamu-A* and *Mamu-B* genes as described previously (31). Briefly, locus-specific reverse transcription-PCR (RT-PCR) products from total cellular RNAs were prepared and used to form heteroduplex DNAs with a 5′ Cy5-labeled reference strand (50). The heteroduplex DNAs were subjected to a 6% nondenaturing acrylamide gel electrophoresis to identify the patterns of MHC-I haplotypes. In addition, although recombination events could not be ruled out, major *Mamu-A* and *Mamu-B* alleles were determined by cloning the RT-PCR products and sequencing at least 48 clones for each locus from each subject as described previously (38). Because we used locus-specific primers in the RT-PCR, which were designed on the basis of known alleles (31, 38), MHC class I alleles harboring mismatches with the primer sequences or alleles of low expression would not be amplified well, hence there was a limitation that not all of the MHC class I alleles could be detected in our study. Confirmed *Mamu-A* and *Mamu-B* alleles in MHC-I haplotypes A, E, B, and

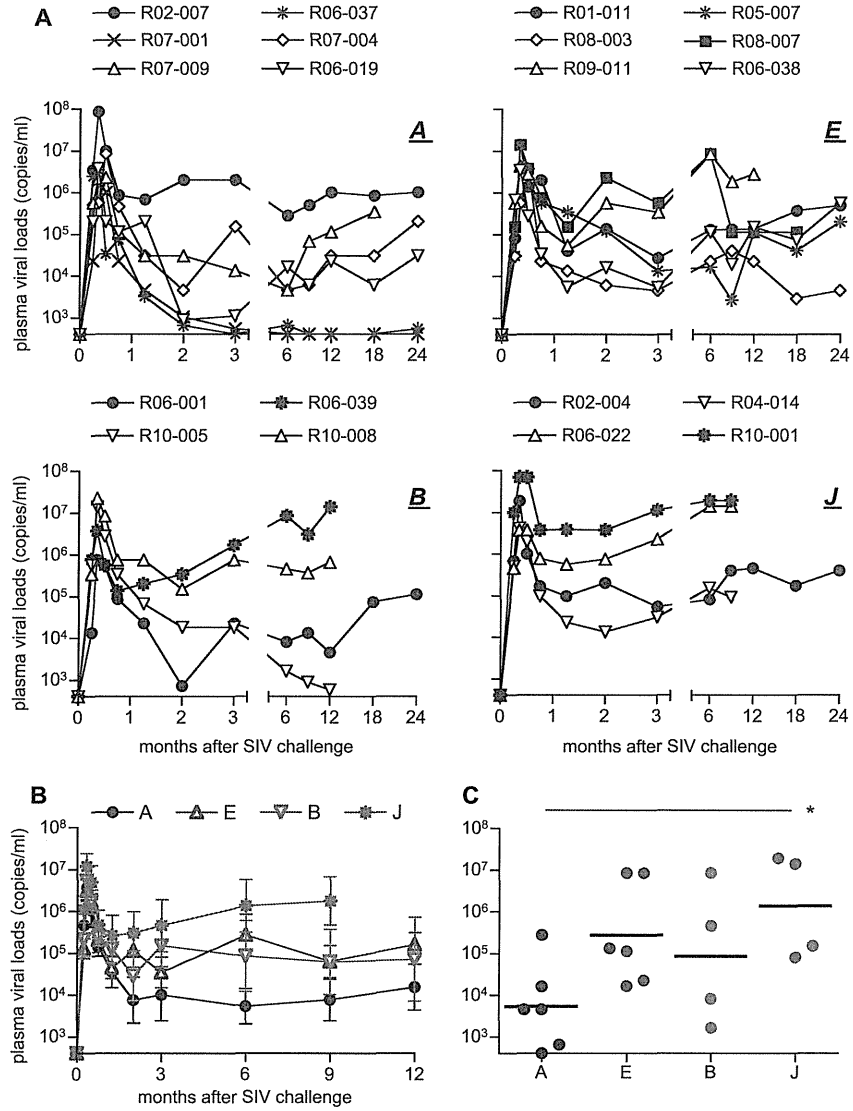

FIG 1 Plasma viral loads after SIVmac239 challenge. Plasma viral loads (SIV *gag* RNA copies/ml plasma) were determined as described previously (31). The lower limit of detection is approximately 4×10^2 copies/ml. (A) Changes in plasma viral loads after challenge in A^+ (upper left), E^+ (upper right), B^+ (lower left), and J^+ (lower right) macaques. (B) Changes in geometric means of plasma viral loads after challenge in A^+ (black), E^+ (blue), B^+ (green), and J^+ (red) animals. (C) Comparison of plasma viral loads at 6 months among four groups. Those of A^+ animals were significantly lower than those of J^+ animals ($P = 0.0444$ by one-way ANOVA and Tukey-Kramer's multiple-comparison test).

J are shown in Table 1 (38). All animals were unvaccinated and challenged intravenously with 1,000 $TCID_{50}$ (50% tissue culture infective doses) of SIVmac239 (22). At 1 week after challenge, macaques R06-019, R06-038, and R10-008 were intravenously infused with 300 mg of nonspecific immunoglobulin G purified from uninfected rhesus macaques (57). Fifteen animals were euthanized when they showed typical signs of AIDS, such as reduction in peripheral $CD4^+$ T-cell counts, loss of body weight, diarrhea, and general weakness. Autopsy revealed lymphoatrophy or postpersistent generalized lymphadenopathy conditions consistent with AIDS (20). All animals were maintained in accordance with the guidelines for animal experiments at the National Institute of Biomedical Innovation and National Institute of Infectious Diseases.

Analysis of SIV antigen-specific $CD8^+$ T-cell responses. SIV antigen-specific $CD8^+$ T-cell responses were measured by the flow-cytometric analysis of gamma interferon (IFN-γ) induction as described previously (17). Peripheral blood mononuclear cells (PBMCs) were cocultured with autologous herpesvirus papioimmortalized B-lymphoblastoid cell lines (B-LCLs) pulsed with peptide pools using panels of overlapping peptides spanning the entire SIVmac239 Gag, Pol, Vif, Vpx, Vpr, Tat, Rev, Env, and Nef amino acid sequences. Intracellular IFN-γ staining was performed using a Cytofix Cytoperm kit (BD, Tokyo, Japan). Fluorescein isothiocyanate-conjugated anti-human CD4 (BD), peridinin chlorophyll protein (PerCP)-conjugated anti-human CD8 (BD), allophycocyanin Cy7 (APC-Cy7)-conjugated anti-human CD3 (BD), and phycoerythrin (PE)-conjugated anti-human IFN-γ antibodies (Biolegend, San Diego, CA) were used. Specific T-cell levels were calculated by subtracting nonspecific IFN-γ^+ T-cell frequencies from those after peptide-specific stimulation. Specific T-cell levels of less than 100 cells per million PBMCs were considered negative. Using PBMCs obtained from four SIV-infected macaques, we compared antigen-specific $CD8^+$ T-cell frequencies measured by this method (using peptide-pulsed B-LCLs) to those measured by the flow-cytometric analysis of IFN-γ induction after a pulse of PBMCs with peptides (without using B-LCLs). The levels of the former tended to be slightly higher than those of the latter. Specific $CD8^+$ T-cell responses, which were shown to be 100 to 200 cells per million PBMCs by the former method using B-LCLs, were undetectable by the latter method.

Sequencing analysis of plasma viral genomes. Viral RNAs were extracted using the High Pure Viral RNA kit (Roche Diagnostics, Tokyo, Japan) from macaque plasma obtained around 1 year after challenge. Fragments of cDNAs encoding SIVmac239 Gag, Pol, Vif, Vpx, Vpr, Tat, Rev, and Nef were amplified by nested RT-PCR from plasma RNAs and subjected to direct sequencing by using dye terminator chemistry and an automated DNA sequencer (Applied Biosystems, Tokyo, Japan) as described before (19). Predominant nonsynonymous mutations were determined. The Env-coding region, which is known to have multiple antibody-related mutations, was not included for the analysis.

Analysis of SIV-specific polyfunctional T-cell responses. To analyze polyfunctionality in SIV-specific T-cell responses, we examined the SIV-specific induction of IFN-γ, tumor necrosis factor alpha (TNF-α), interleukin-2 (IL-2), macrophage inflammatory protein 1β (MIP-1β), and CD107a in $CD4^+$ and $CD8^+$ T cells as described previously (58), with some modifications. Around 8 months after challenge, PBMCs were cocultured with B-LCLs infected with vesicular stomatitis virus G protein-pseudotyped SIVGP1 for the SIV-specific stimulation or mock-infected B-LCLs for nonspecific stimulation. The pseudotyped virus was obtained by the cotransfection of 293T cells with a vesicular stomatitis virus G protein expression plasmid and an *env* and *nef* deletion-containing simian-human immunodeficiency virus molecular clone (SIVGP1) DNA that has the genes encoding SIVmac239 Gag, Pol, Vif, Vpx, and a part of Vpr (31, 46). Immunostaining was performed using a Fix & Perm fixation and permeabilization kit (Invitrogen, Tokyo, Japan) and the following monoclonal antibodies: APC-Cy7-conjugated anti-human CD3 (BD), PE-Texas red-conjugated anti-human CD4 (Invitrogen), Alexa Fluor 700-conjugated anti-human CD8 (BD), PE-Cy7-conjugated anti-human IFN-γ (eBioscience, San Diego, CA), Pacific blue-conjugated anti-human TNF-α (Biolegend), PerCP-Cy5.5-conjugated anti-human IL-2 (Biolegend), PE-conjugated anti-human MIP-1β (BD), and Alexa Fluor 647-conjugated anti-human CD107a (Biolegend). Dead cells were stained using Live/Dead Fixable Dead Cell Stain kit (Invitrogen). Analysis was carried out using PESTLE (version 1.6.1) and SPICE (version 5.2) programs as described previously (42). The polyfunctionality (polyfunctional value) was shown as mean numbers of induced factors among the five (IFN-γ, TNF-α, IL-2, MIP-1β, and CD107a) per SIV-specific T cell.

Statistical analysis. Statistical analyses were performed using R software (R Development Core Team). Comparisons were performed by one-way analysis of variance (ANOVA) and Tukey-Kramer's multiple comparison test with significance levels set at $P < 0.05$. Correlation was analyzed by the Pearson test.

TABLE 2 List of macaques in this study

MHC-I haplotype	Macaque	Disease progression	Euthanasia time point (mo)
A	R02-007	AIDS	42
A	R06-037	No	49
A	R07-001	No	49
A	R07-004	AIDS	40
A	R07-009	AIDS	17
A	R06-019	AIDS	43
E	R01-011	AIDS	24
E	R05-007	AIDS	37
E	R08-003	Under observation (24 months)	
E	R08-007	AIDS	20
E	R09-011	AIDS	12
E	R06-038	AIDS	22
B	R06-001	AIDS	34
B	R06-039	AIDS	13
B	R10-005	Under observation (12 months)	
B	R10-008	Under observation (12 months)	
J	R02-004	AIDS	37
J	R04-014	AIDS	9
J	R06-022	AIDS	5
J	R10-001	AIDS	9

RESULTS

SIV infection in Burmese rhesus macaques. We accumulated four groups of unvaccinated, SIVmac239-infected Burmese rhesus macaques, groups A^+ ($n = 6$), E^+ ($n = 6$), B^+ ($n = 4$), and J^+ ($n = 4$), sharing MHC-I haplotypes A (*90-120-Ia*), E (*90-010-Ie*), B (*90-120-Ib*), and J (*90-088-Ij*), respectively, to compare SIV infections among these groups (Table 1). Out of these 20 animals, 18 showed persistent viremia (geometric mean plasma viral loads at 6 months of 1.6×10^5 copies/ml), while in the remaining two (A^+ macaques R06-037 and R07-001), plasma viral loads became less than 10^3 copies/ml or were undetectable at the set point (Fig. 1A). The former 18 animals are referred to as noncontrollers and the latter two as controllers in this study. Fifteen noncontrollers were euthanized with AIDS progression in 4 years (geometric mean survival period of 24 months), and the remaining three, after 1 or 2 years, are under observation (Table 2).

Group A^+ macaques, including two controllers, showed lower set point viral loads, whereas group J^+ macaques had higher viral loads (Fig. 1B). Viral loads in group E^+ and B^+ macaques were at intermediate levels. Multiple comparisons indicated significant